

# Accepted Manuscript

Southward extension of the Bangonghu–Nujiang Suture: Evidence from Early Cretaceous intermediate and felsic magmatism in the Gaoligong Orogen, China

Xuexiang Qi, Cheng Wei, Chao Zhang, Shiqi Zhang, Zhaochu Hu, Fengbao Ji

PII: S1367-9120(18)30392-4

DOI: <https://doi.org/10.1016/j.jseaes.2018.09.007>

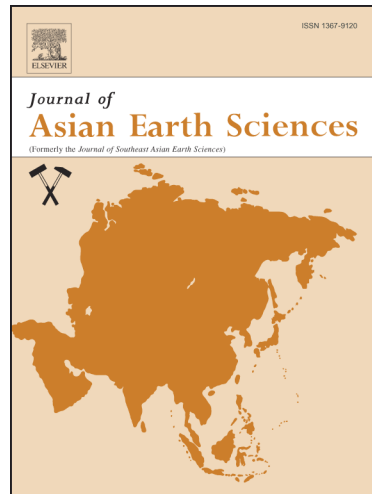
Reference: JAES 3644

To appear in: *Journal of Asian Earth Sciences*

Received Date: 22 September 2017

Revised Date: 5 September 2018

Accepted Date: 8 September 2018



Please cite this article as: Qi, X., Wei, C., Zhang, C., Zhang, S., Hu, Z., Ji, F., Southward extension of the Bangonghu–Nujiang Suture: Evidence from Early Cretaceous intermediate and felsic magmatism in the Gaoligong Orogen, China, *Journal of Asian Earth Sciences* (2018), doi: <https://doi.org/10.1016/j.jseaes.2018.09.007>

This is a PDF file of an unedited manuscript that has been accepted for publication. As a service to our customers we are providing this early version of the manuscript. The manuscript will undergo copyediting, typesetting, and review of the resulting proof before it is published in its final form. Please note that during the production process errors may be discovered which could affect the content, and all legal disclaimers that apply to the journal pertain.

**Southward extension of the Bangonghu–Nujiang Suture: Evidence  
from Early Cretaceous intermediate and felsic magmatism in the  
Gaoligong Orogen, China**

Xuexiang Qi<sup>a</sup>, Cheng Wei<sup>a</sup>, Chao Zhang<sup>b</sup>, Shiqi Zhang<sup>a</sup>, Zhaochu Hu<sup>c</sup>, Fengbao Ji<sup>a</sup>

<sup>a</sup> *Institute of Geology, Chinese Academy of Geological Sciences, Beijing 100037, China*

<sup>b</sup> *Tianjing Institutes of Geology and Mineral Resources, CGS, Nanjing 210016, China*

<sup>c</sup> *State Key Laboratory of Geological Processes and Mineral Resources, Chinese University of Geosciences, Wuhan 430074, China*

**Corresponding author: Xuexiang Qi**

**Institute of Geology, CAGS,  
No. 26 Baiwanzhuang Road,  
Beijing 100037, China  
Fax: +86 10 68994781**

**E-mail: qxuex2005@163.com (X. X. Qi)**

## Abstract

It remains debated as to whether the Gaoligong Orogen between the Tengchong and Baoshan blocks in Yunnan, China, is the southward extension of the Tibetan Bangonghu–Nujiang Suture (BNS). Here we present new geochronological and petrochemical data for Early Cretaceous magmatic rocks of the Gaoligong Orogen. The LA–ICP–MS U–Pb dating of zircons from diorites, granodiorites, and granites yielded weighted mean  $^{206}\text{Pb}/^{238}\text{U}$  ages of 120–118, 128–122, and 109–128 Ma, respectively. For the diorites, the  $\varepsilon_{\text{Hf}}(t)$  values of zircons fall in a range of +1.2 to +5.4 with  $T_{\text{DM}}^{\text{C}}$  ages of 744–979 Ma, for the granodiorites they fall in a range of –9.8 to +2.9 with  $T_{\text{DM}}^{\text{C}}$  ages of 888–1564 Ma, and for the granites the range is –8.0 to –1.1 with  $T_{\text{DM}}^{\text{C}}$  ages of 1101–1488 Ma. They are magnesian, calc-alkaline, enriched in LILEs and LREEs, and have strong negative Nb, Ta, P, and Ti anomalies and high values of Mg<sup>#</sup>. All these features are indicative of continental arc affinities. The data suggest that the dioritic and granitic magmas were produced by the mixing of variable proportions of mantle- and crust-derived magmas at an active continental margin. The ages and tectonic settings of the diorites, granodiorites, and granites are similar to rocks found within the BNS. Considering the ophiolitic mélange belt, the Middle Jurassic basaltic magmatism, and the marine-facies stratigraphic features of the Gaoligong Orogen are very similar to features in the BNS, we conclude that the Gaoligong Orogen represents the suture between the Tengchong and Baoshan blocks, and is the southward extension of the BNS.

**Key words:** zircon U–Pb geochronology; geochemistry; intermediate and felsic magmatism; Gaoligong Orogen; Bangonghu–Nujiang Suture.

## 1. Introduction

The Bangong–Nujiang Suture (BNS) in Tibet runs east–west and forms a major

Tethyan suture on the Tibetan Plateau, separating the Qiangtang Block in the north from the Lhasa Block in the south (Fig. 1). A discontinuous belt of Jurassic to Early Cretaceous ophiolitic rocks, calc-alkaline arc magmatic rocks, and high- to ultrahigh-pressure metamorphic rocks in central Tibet indicate that the Tethyan oceanic lithosphere was subducted northwards under the South Qiangtang block during the Middle Triassic to Middle Jurassic (e.g., Coulon et al., 1986; Yin and Harrison, 2000; Kapp et al., 2003, 2007; Guynn et al., 2006; Zhang et al., 2012, 2014, 2017) and southwards under the North Lhasa block during the Middle Jurassic to Early Cretaceous (e.g., Hsü et al., 1995; Pan et al., 2006; Zhu et al., 2009, 2013, 2015; Qi et al., 2011; Fan et al., 2015). However, around the Eastern Himalayan Syntaxis, the southward extension of the BNS remains debated. Liu et al. (2016) considered the Myitkyina ophiolite belt in Myanmar to be the southern continuation of the Bangonghu–Nujiang Meso-Tethyan suture because of their similar Middle Jurassic ages (ca. 173 Ma), and they considered the Tengchong Block in SW Yunnan to be a segment of the Sibumasu Block that is linked with the Qiangtang Block (e.g., Wopfner, 1996; Liu et al., 2006; Metcalfe, 2013; Metcalfe and Aung, 2014). However, this contradicts the model of Mitchell (1993), who proposed that the Myitkyina ophiolite belt represents a truncated northerly extension of the Kalaymyo ophiolite belt as part of a single suture that connects with the Yarlung–Tsangpo Suture, and that the Myitkyina ophiolite belt has been offset in the south by movement on the Sagaing Fault (Fig. 1b). The Early Cretaceous granites exposed in the eastern part of the Tengchong Block and in Bomi–Chayu are related to the subduction of the Bangong–Nujiang oceanic lithosphere (e.g., Qi et al., 2011; Ma et al., 2014; Wang et al., 2014, 2015; Zhu et al., 2015; Xie et al., 2016; Zhao et al., 2017). Accordingly, others have argued that the Gaoligong tectonic zone is a suture zone that separates the Tengchong Block in the west from the Baoshan Block in the east (Fig. 1), and represents the southerly extension of the BNS (e.g., Qi et al., 2011; Xu et al., 2012, 2015; Ma et al., 2014; Wang et al., 2014, 2015; Zhu et al., 2015; Xie et al., 2016; Zhao et al., 2017). In which case, the Tengchong Block should be linked with the Lhasa Block rather than the Sibumasu Block (e.g., Shi et

al., 2008; Wopfner and Jin, 2009; Zhang et al., 2013; Liao et al., 2015; Qi et al., 2015; Xie et al., 2016).

Previous research in the Gaoligong Orogen has focused on the Early Cretaceous granitic rocks along the eastern margin of the Tengchong Block (Fig. 2), and it has been suggested that the magmatic belt is related to crustal thickening that resulted from collision between the Lhasa–Tengchong and Qiangtang -Baoshan blocks based on the S-type granites with negative zircon  $\varepsilon_{\text{Hf}}(t)$  values (e.g., Xu et al., 2012). However, there are more I-type granites with high-K, calc-alkaline, and positive to negative zircon  $\varepsilon_{\text{Hf}}(t)$  values (e.g., Qi et al., 2011; Zhu et al., 2015; Xie et al., 2016) and diorites besides S-type granites which bear strong similarities in lithology, ages, geochemistry to those in the northern Lhasa block(e.g., Zhu et al., 2009, 2011; Qi et al., 2011; Xu et al., 2012; Xie et al., 2016 ), that the belt represents a continental arc resulted from southward subduction of the Bangong–Nujiang oceanic slab (e.g., Zhu et al., 2009, 2011, 2015; Qi et al., 2011; Zhao et al., 2016; Xie et al., 2016). Here, we provide the first report on all the Early Cretaceous diorites and granites along the eastern margin of the Gaoligong Orogen (Fig. 2), using new geochemical as well as precise LA–ICP–MS U–Pb zircon ages and Hf isotopic compositions. We then elucidate the relationships between these rocks and subduction and collision, and trace the southward extent of the Bangonghu–Nujiang Suture.

## 2. Geologic setting

The Gaoligong Orogen is a N–S trending mountain range that bends in an arcuate fashion towards the Mogok metamorphic belt in the south, with the Sagaing Fault defining the tectonic boundary between these two bodies (Figs. 1b, 2). The orogen comprises a ~400 km long and ~20 km wide high-grade metamorphic belt and Early Cretaceous magmatic belt in the eastern Tengchong Block. The high-grade metamorphic belt consists of a sequence of greenschist- and amphibolite-facies metasedimentary and meta-intrusive rocks, such as orthogneiss, paragneiss, schist,

quartzite and marble. Parts of them have been mylonitized and show a subvertical foliation and subhorizontal stretching lineation. To the west, the metamorphic belt is overlain by Neogene clastic deposits, while to the east it is bordered by Paleozoic and Mesozoic sediments of the Baoshan Block, from which it is separated by the Lushui–Longling–Ruili dextral shear zone (LLRZ). The rocks of the high-grade metamorphic belt have yielded zircon U–Pb ages of 518–460 Ma (e.g., Li et al., 2012; Cai et al., 2013; Eroğlu et al., 2013; Wang et al., 2013; Zhao et al., 2016), whereas the recently recognized and widely distributed granitic plutons of the orogen have yielded zircon U–Pb ages of 131–114 Ma (e.g., Yang et al., 2006; Chiu et al., 2009; Ji et al., 2009; Zhu et al., 2009, 2015; Cong et al., 2011; Qi et al., 2011; Xu et al., 2012; Xie et al., 2016). A belt of tectonic mélange (ca. 130 km long and 3–5 km wide) has been identified within the southeastern margin of the Gaoligong Orogen (e.g., Tan and Zhan, 1990; Liu et al., 2002; Yin et al., 2012) (Fig. 2), and it consists of abyssal facies flysch sedimentary rocks with siliceous rock and tectonic slices of serpentine peridotite, basalt, gabbro/diabase, chert, paragneiss, and Paleozoic marble and dolomite. Although Chu et al. (2009) considered the Santaishan slices of serpentine peridotite was derived from old sub-continental lithospheric mantle (e.g., Zhang, 2014) based on the high initial  $^{87}\text{Sr}/^{86}\text{Sr}$ , low initial  $\varepsilon_{\text{Nd}}$  and  $\gamma_{\text{Os}}$ , and Os isotopic model ages ( $t_{\text{RD}}=0.97\text{--}1.71\text{ Ga}$ ), it is still an ophiolite belt representing a suture. The reasons are as fellow: 1) The rock assemblage of the mélange is consistent with the ophiolite in BNS; 2) These old continental lithospheric mantle ultrabasic rocks also exists in Tethyan ophiolite belt, such as the peridotites from the Dongqiao ophiolite ( $t_{\text{RD}}=1.5\text{--}2.2\text{ Ga}$ , Shi et al., 2012), peridotites from the External Liguride in Bangong-Nujiang ophiolite with Sr and Nd model ages of 2.4 Ga (e.g., Rampone et al., 1995), peridotites from the Yungbwa in Yarlung Tsangpo ophiolite belt ( $t_{\text{RD}}=1.0\text{ Ga}$ , Liu et al., 2012), which were exposed on the sea floor, had heterogeneous isotope compositions and contained some ancient mantle domains during the early stages of the opening of the Tethys ocean basin (e.g., Rampone et al., 1995; Liu et al., 2012; Shi et al., 2012), or resulted from the subduction of oceanic crust and overlying sediments into the convective upper

mantle (e.g., Martin, 1994; Büchl et al., 2004).

The Tengchong Block is bordered by the Gaoligong metamorphic belt in the east and the Myitkyina suture in the west (Fig. 1b). Although the age of ophiolite (169-171Ma) is consistent with that in the BNS (e.g., Yang et al., 2012; Liu et al., 2016), the Myitkyina suture is considered the equivalent of the Yarlung–Tsangpo Suture, and it separates rocks related to India in the west from rocks related to the Tengchong (Burma) Block in the east (e.g., Mitchell, 1993; Yang et al., 2012; Xu et al., 2015), because this Jurassic ophiolites exist also in Yarlung Tsangpo suture, and the spatial and temporal variations and changing magmatic compositions over time in the Tengchong block closely resemble those of the Lhasa block and differ notably from those of the South Qiangtang block (e.g., Zhu et al., 2009, 2011, 2015; Qi et al., 2011, 2015; Zhao et al., 2016; Xie et al., 2016) . The Tengchong Block is therefore thought to continue northwards into the Lhasa Block, which was bent around the eastern Himalayan syntaxis (e.g., Searle et al., 2007). Rocks of the Tengchong Block comprise greenschist- and amphibolite- facies gneiss, weakly metamorphosed upper Paleozoic sediments, and upper Mesozoic to lower Cenozoic granites and mafic dikes. In the last 5.5 Myr, a number of active basaltic and andesitic volcanoes eruptions had occurred in the Tengchong Block (e.g., Zhu et al., 1983; Wang et al., 2007; Zhou et al., 2012).

The Baoshan Block is the northward continuation of the Sibumasu Block, which was detached from the northern margin of Gondwana during the Sakmarian (e.g., Metcalfe, 2002). Following the closure of the Paleo-Tethys, the block was welded to the Indochina Block along the Lancangjiang Suture during the Triassic (e.g., Metcalfe, 2002) (Fig. 1), but the correlation of the Baoshan and Tengchong blocks during late Mesozoic is debated. The Baoshan Block consists of Cambrian to Jurassic marine deposits (metamorphosed to low–medium grades), Permian volcanics, and Quaternary conglomerates and sandstones. The Carboniferous deposits are mainly glacio-marine diamictites in the lower parts and siltstones in the upper part. The early Permian Woniusi Basalts (basalts and basaltic volcaniclastics) are thought to be related to the rifting of the Sibumasu Block from Gondwana (e.g.,

Ali et al., 2013; Liao et al., 2015).

### 3. Samples and petrography

The samples analyzed in this study were collected from 10 plutons (diorites, granodiorites, and granites) that were emplaced during the Early Cretaceous (Fig. 2). The diorite samples ( $\delta_1$  and  $\delta_2$ ) are sampled from the western Lushui and southern Lianghe, respectively. The  $\delta_1$  is a long elliptical body, about 4km long, 1.5km wide and approximately 5km<sup>2</sup> in extent, and intrudes into the mylonitonal gneiss. The  $\delta_2$  is also a long elliptical intrusion, about 5km long, 2km wide and approximately 7km<sup>2</sup> in area, and shows intrusive contacts with Gaoligong formation metamorphic rock. The three plutons of granodiorite ( $\gamma\delta_1$  to  $\gamma\delta_3$ ) are located to the north and west of Longling, and to the northeast of Ruili. They are all long strip intrusions, about 10-12km long, 1-2km wide, and approximately 8-13km<sup>2</sup> in extend, and shows intrusive contacts with the mylonitonal gneiss. The five granite plutons ( $\gamma_1$  to  $\gamma_5$ ) occur at the Gaoligong ductile shear zone, they are all long strip intrusions, with 3-12km long, 0.5-1.5km wide and approximately 1-10km<sup>2</sup> in area, and were emplaced within the high-grade metamorphic rocks.

#### 3.1. Diorites

The diorites, reported here for the first time, are divided into monzodiorite ( $\delta_1$ ) and gabbroic diorite ( $\delta_2$ ). The monzodiorite is a fine-grained rutile-bearing metadiorite with a gneissic structure. The dominant minerals are biotite (30%), hornblende (20%), plagioclase (31%), and K-feldspar (15%), together with accessory titanite (3%), rutile (1%), and minor zircon. Plagioclase and K-feldspar occur generally as subhedral to euhedral laths. The hornblende occurs as anhedral laths, and it exhibits a pleochroism from yellowish-green to a deep blue-green. Titanite and rutile occur either as euhedral granular inclusions in hornblende and biotite, or as

interstitial aggregates of small granular grains. The weak foliation is defined by the orientation of biotite and hornblende. The gabbroic diorite is coarse-grained, and the dominant minerals are hornblende (50%), plagioclase (42%), and K-feldspar (8%). Accessory phases are magnetite, zircon, and apatite. The plagioclase and K-feldspar occur generally as subhedral to anhedral laths that have been weakly altered to sericite and kaolinite, respectively. Hornblende occurs as anhedral prisms that exhibit a pleochroism from yellowish-green to deep blue-green. Most of the hornblende grains have residual cores of pyroxene (Fig. 3a, b).

### 3.2. Granodiorites

The three plutons of granodiorite ( $\gamma\delta_1$  to  $\gamma\delta_3$ ) are medium- to coarse-grained and gneissose. The dominant minerals are plagioclase (30%–35%), K-feldspar (20%–30%), quartz (25%–30%), hornblende (4%–25%), and biotite (5%–12%), and the accessory phases are magnetite, zircon, allanite, and titanite. Plagioclase and K-feldspar occur generally as subhedral to anhedral laths, and have been partly altered to sericite and kaolinite, respectively. Quartz occurs as anhedral grains or as interstitial fine-grained granular aggregates. The hornblende forms subhedral to anhedral prisms that are pleochroic from yellowish-green to deep blue-green. The biotite is anhedral and pleochroic from yellowish-green to brownish color. Allanite occurs as euhedral prisms, but only in samples 15QML-57 to -61, and these samples also contain 2% to 3% more titanite than other samples. The weak foliation is defined by the orientation of biotite, hornblende, and feldspar. Mafic microgranular enclaves (MMEs) occur in these granodiorites, and are randomly distributed. Their shapes vary from irregular to ellipsoidal or round, and their sizes range from 5 to 20 cm. The MMEs have transitional contact zones with their host granodiorite, and they have halos of felsic leucosome up to 1 cm thick (Fig. 3c). The MMEs are dark green, equigranular, and fine-grained, and have typical igneous textures without cumulate textures (Fig. 3d). The main phases in the MMEs are hornblende (45%), K-feldspar (20%), plagioclase (30%), and spinel (5%), and the accessory phases are

magnetite, zircon, and titanite. The minerals in the MMEs are much smaller (0.2 to 0.3 mm) than those in the host granodiorite (1.0 to 2.0 mm).

### 3.3. Granites

The five granite plutons ( $\gamma_1$  to  $\gamma_5$ ) consist of medium- to coarse-grained biotite-bearing porphyritic granites with a gneissic structure. The dominant minerals are plagioclase (20%–32%), K-feldspar (25%–30%), quartz (30%–40%), and biotite (8%–12%), and the accessory phases are zircon, titanite, and garnet. Plagioclase and K-feldspar occur generally as subhedral to anhedral laths, and some of the grains form relatively coarse (1–2 cm) phenocrysts. Quartz occurs as anhedral grains or as interstitial fine-grained granular aggregates. The biotite is anhedral and pleochroic from yellowish-green to a brownish color. The foliation is defined by the orientation of biotite and feldspar in the groundmass. Garnet was observed only in samples 15QML-5 to -9, where it forms euhedral grains.

## 4. Analytical methods

Whole-rock major and trace elements were analyzed at the National Research Center for Geoanalysis (NRCG), CAGS. Major element oxides were determined using ICP-AES (PE8300). The analytical uncertainty was <0.5%. The trace elements and the rare earth elements (REE) were analyzed by ICP-MS (PE300D). The analytical uncertainties were 1%–5% for abundances greater than 1 ppm, and 5%–10% for abundances less than 1 ppm. The effective digit for the trace elements and rare earth elements is 3 bits.

The zircons were separated from whole-rock samples by a combination of density techniques and handpicking under an electron microscope. The grains were mounted in epoxy, polished to about half of their thickness, and photographed in transmitted and reflected light. Cathodoluminescence (CL) imaging of the zircon

grains was carried out using scanning electron microprobes at the Beijing SHRIMP Center of the Chinese Academy of Geological Sciences (CAGS). The U–Pb dating of the zircons was performed by laser ablation–inductively coupled plasma–mass spectrometry (LA–ICP–MS), and the zircon Lu–Hf isotope analyses were carried out *in situ* by using a new wave UP213 laser–ablation microprobe, attached to a Neptune multi-collector ICP–MS at the State Key Laboratory of Geological Processes and Mineral Resources, Faculty of Earth Sciences, China University of Geosciences (Wuhan). The analytical methods and procedures have been described by Hu et al. (2012) and Qi et al. (2012).

## 5. Results

### 5.1. Whole-rock major and trace element geochemistry

#### 5.1.1. Diorites

The gabbroic-diorites and monzodiorites (Fig. 4a) are characterized by low contents of SiO<sub>2</sub> (50.95–54.16 wt.%) and K<sub>2</sub>O (0.54–2.34 wt.%), and high contents of CaO (7.01–9.60 wt.%) (Table 1). The Al<sub>2</sub>O<sub>3</sub> contents vary from 15.21 to 16.71 wt.%, and A/NK ratios [A/CNK = molecular Al<sub>2</sub>O<sub>3</sub>/(Na<sub>2</sub>O + K<sub>2</sub>O)] and A/CNK ratios [A/CNK = molecular Al<sub>2</sub>O<sub>3</sub>/(CaO + Na<sub>2</sub>O + K<sub>2</sub>O)] range from 2.04 to 3.22 and 0.70 to 0.77 respectively, indicating the rocks are metaluminous. The values of Mg<sup>#</sup> [Mg<sup>#</sup> = 100 × molar Mg<sup>2+</sup>/(Mg<sup>2+</sup> + total Fe<sup>2+</sup>)] range from 52.9 to 69.5. The Na<sub>2</sub>O + K<sub>2</sub>O vs. SiO<sub>2</sub>, FeO/(FeO+MgO) vs. SiO<sub>2</sub>, Na<sub>2</sub>O + K<sub>2</sub>O-CaO vs. SiO<sub>2</sub> and K<sub>2</sub>O vs. SiO<sub>2</sub> diagrams (Fig. 4) show all samples are subalkaline and belong to the magnesian, calcic to alkali-calcic series (e.g., Arculus, 2003; Frost et al., 2001). The TiO<sub>2</sub> contents for samples 15QLP-39 to -43 range from 2.24 to 2.30 wt.%, higher than in samples 15QML-65 to -69 (0.80–1.44 wt.%); these variable contents can be related to the high contents of titanite (3%) and rutile (1%) in the monzodiorites.

The chondrite-normalized rare earth element (REE) patterns (Fig. 5a) indicate that the two dioritic plutons are weakly enriched (LREE/HREE ratios = 3.54–6.57) with a

weak fractionation of LREEs over HREEs and with  $(\text{La}/\text{Sm})_{\text{N}} = 1.95\text{--}2.25$  [where N denotes normalization to the chondrite values of Sun and McDonough (1989)]. Negative Eu anomalies ( $\text{Eu}/\text{Eu}^* = 0.79\text{--}0.94$ ) are weak or lacking. Primitive-mantle-normalized spider diagrams (Fig. 5b) show that the rocks are enriched in large ion lithophile elements (LILEs) such as Th, U, Ba, K, and Rb, and LREEs, including La and Ce, relative to primitive mantle. The monzodiorites and gabbroic diorites respectively show weak to strong negative anomalies of Nb, Ta, P, and Ti.

### 5.1.2. Granodiorites

The three granodiorites are characterized by  $\text{SiO}_2$  contents of 63.54–70.85 wt.%,  $\text{K}_2\text{O}$  contents of 1.58 to 4.85 wt.%,  $\text{Na}_2\text{O}$  of 3.03 to 4.37 wt.%, and  $\text{CaO}$  of 3.11 to 4.58 wt.% (Table 1). The  $\text{Al}_2\text{O}_3$  contents vary from 15.20 to 17.00 wt.%, and A/NK ratios and A/CNK ratios range from 1.58 to 2.06 and 0.93 to 1.10, respectively, indicating metaluminous compositions. The values of  $\text{Mg}^{\#}$  ranges from 38.3 to 52.3. The  $\text{Na}_2\text{O} + \text{K}_2\text{O}$  vs.  $\text{SiO}_2$ ,  $\text{FeO}/(\text{FeO}+\text{MgO})$  vs.  $\text{SiO}_2$ ,  $\text{Na}_2\text{O} + \text{K}_2\text{O}-\text{CaO}$  vs.  $\text{SiO}_2$  and  $\text{K}_2\text{O}$  vs.  $\text{SiO}_2$  diagrams show all samples belong to the magnesian, medium- to high-K calc-alkaline series (Fig. 4), and they have Cordilleran-type magmatic features (e.g., Frost et al., 2001).

The chondrite-normalized REE patterns and primitive-mantle-normalized spider diagram show that the granodiorites have significantly fractionated LREE and relatively flat HREE patterns with weak to moderate negative Eu anomalies ( $\text{Eu}/\text{Eu}^* = 0.49\text{--}0.86$ , except for two samples of 1.04 to 1.17) (Fig. 5c), strong enrichments in Ba, K, Rb, and LREEs, including La and Ce, relative to primitive mantle, and significantly negative anomalies of Ba, Nb, Ta, P, and Ti relative to neighboring elements. Sr also displays negative anomalies except in samples 15QML-57 to -61, which show positive anomalies (Fig. 5d) due to the high contents of titanite (2%–3%).

### 5.1.3. Granites

The granitic intrusions have relatively high contents of  $\text{SiO}_2$  (69.62–76.49 wt.%), relatively low  $\text{Al}_2\text{O}_3$  contents (12.46–15.77 wt.%),  $\text{CaO}/\text{Na}_2\text{O}$  ratios of 0.36 to 0.98 (average 0.58),  $\text{K}_2\text{O}$  contents of 3.27 to 5.60 wt.%, and  $\text{Na}_2\text{O}$  contents of 2.29 to 3.36 wt.% (Table 1). Samples 15QML-5 to -9 have  $\text{A/NK}$  ratios of 1.11–1.25,  $\text{A/CNK}$  ratios of 1.28 to 1.55, and are peraluminous, but the other granitic samples have metaluminous compositions with  $\text{A/NK}$  ratios and  $\text{A/CNK}$  ratios ranging from 1.36 to 1.61 and 0.97 to 1.08, respectively. The values of  $\text{Mg}^{\#}$  range from 35.9 to 51.3. The  $\text{Na}_2\text{O} + \text{K}_2\text{O}$  vs.  $\text{SiO}_2$ ,  $\text{FeO}/(\text{FeO}+\text{MgO})$  vs.  $\text{SiO}_2$ ,  $\text{Na}_2\text{O} + \text{K}_2\text{O}-\text{CaO}$  vs.  $\text{SiO}_2$  and  $\text{K}_2\text{O}$  vs.  $\text{SiO}_2$  diagrams (Fig. 4) show all samples belong to the magnesian, high-K calc-alkaline series, and they have Cordilleran-type magmatic features (e.g., Frost et al., 2001).

The chondrite-normalized REE patterns are characterized by an enrichment in LREEs relative to HREEs with  $(\text{La}/\text{Sm})_{\text{N}}$  varying from 3.72 to 6.53, and strong negative Eu anomalies with  $\text{Eu}/\text{Eu}^*$  varying from 0.27 to 0.54 (Fig. 5e). The primitive-mantle-normalized spider diagrams (Fig. 5f) show that relative to primitive mantle these rocks are characterized by strong enrichments in LILEs such as Rb, Ba, and K, radiogenic product-heat elements (RHEs) such as U and Th, and LREEs, and the diagrams display distinct negative anomalies in Ba, Sr, Nb, Ta, P, and Ti relative to neighboring elements.

### 5.2. Zircon geochronology

The U–Pb and Lu–Hf isotope data for the zircons from the 10 intrusions are listed in Tables 2 and 3, and representative CL images of the zircons are shown in Fig. 6. The zircons display well-developed short euhedral prismatic forms. Zircons from the diorites have average crystal lengths of 80 to 100  $\mu\text{m}$  and length-to-width ratios of 1.0 to 1.5, while those from the granitoids are 100–200  $\mu\text{m}$  long with length-to-width ratios of 1.5–2.0. All grains from the diorites have indistinct fine oscillatory zoning,

with no indication of resorption or inherited cores, and most of the grains from the granitoids show clearly developed oscillatory zoning with no indication of resorption or inherited cores, except for the zircons from sample 15QQML-83.

The zircons from the diorites, granodiorites, and granites show relatively wide ranges of U (178–5444, 185–5414, and 228–3983 ppm, respectively) and Th (193–11300, 180–2956, and 140–7982 ppm, respectively) contents. The Th/U ratios of all the zircons are greater than 0.1. These ratios and the observed magmatic zoning indicate that the zircons are of magmatic origin (e.g., Hoskin and Schaltegger, 2003). Their U–Pb ages therefore represent the timing of crystallization of the zircons in the granitoid and diorite magmas.

### 5.2.1. Diorites

Samples 15QLP-9 and 15QML-65 were collected from the monzodiorite ( $\delta_1$ ) and gabbroic diorite ( $\delta_2$ ) (Fig. 2), respectively. Twenty-two analyses of 22 zircons from sample 15QLP-9 form a cluster on the concordia curve (Fig. 7a) with a weighted mean  $^{206}\text{Pb}/^{238}\text{U}$  age of  $118 \pm 2.1$  Ma (MSWD = 8.5). Two grains yielded older  $^{206}\text{Pb}/^{238}\text{U}$  ages of  $373 \pm 3.1$  and  $129 \pm 2.1$  Ma (Table 2), and these data were rejected from the age calculations. Twenty analyses of 20 zircons from 15QML-65 were conducted. Among these analyses, three (spots 1, 2, and 3) are strongly discordant, thus setting them apart from the cluster on the concordia curve. The other 17 analyses yield a weighted mean  $^{206}\text{Pb}/^{238}\text{U}$  age of  $120 \pm 2.0$  Ma (MSWD = 3.5) (Fig. 7b), and we interpret this to be the crystallization age of the monzodiorite and gabbroic diorite.

### 5.2.2. Granodiorites

Samples 15QMH-1, 15QLL-21, and 15QML-57 were collected from the granodiorite plutons  $\gamma\delta_1$ ,  $\gamma\delta_2$ , and  $\gamma\delta_3$  (Fig. 2). Twenty-two analyses of 22 zircons from sample 15QMH-1 were conducted. One discordant zircon was rejected from the age

calculation. The other 21 concordant analyses form a tight cluster on the concordia curve with a weighted mean  $^{206}\text{Pb}/^{238}\text{U}$  age of  $122 \pm 1.9$  Ma (MSWD = 4.7) (Fig. 7c). Twenty-two analyses on 22 zircons from sample 15QLL-21 were conducted. Among these, one analysis (spot 19) yielded an age at  $144 \pm 3.1$  Ma, and another (spot 14) yielded an age of  $114 \pm 3.1$  Ma (Table 2). These two ages are slightly older and younger than those of the main zircon population, respectively, and they were therefore excluded from the age calculation. The other 20 analyses yielded a weighted mean  $^{206}\text{Pb}/^{238}\text{U}$  age of  $128 \pm 1.9$  Ma (MSWD = 4.1) (Fig. 7d). Twenty analyses of zircons from sample 15QML-57 were concordant and yielded a weighted mean  $^{206}\text{Pb}/^{238}\text{U}$  age of  $122 \pm 1.7$  Ma (MSWD = 2.8) (Fig. 7e). We interpret these weighted mean  $^{206}\text{Pb}/^{238}\text{U}$  ages of  $122 \pm 1.9$ ,  $128 \pm 1.9$ , and  $122 \pm 1.7$  Ma to represent the crystallization ages of the three granodiorites.

### 5.2.3. Granites

Samples 10QTG-42, 15QML-5, 15QML-83, 15QLR-4, and 15QLM-37 were collected from the granitic plutons  $\gamma_1$  to  $\gamma_5$  (Fig. 2). Twenty analyses on 20 zircons from sample 10QTG-42 are concordant. Three grains yielded slightly older  $^{206}\text{Pb}/^{238}\text{U}$  ages of  $132 \pm 1.6$ ,  $133 \pm 1.6$ , and  $134 \pm 1.3$  Ma (Table 2), setting them apart from the cluster on the concordia curve. The other 17 analyses yield a weighted mean  $^{206}\text{Pb}/^{238}\text{U}$  age of  $121 \pm 2.0$  Ma (MSWD = 8.9) (Fig. 7f). The U–Pb data for 26 zircons from sample 15QML-5 are concordant, forming a tight cluster on the concordia curve with a weighted mean  $^{206}\text{Pb}/^{238}\text{U}$  age of  $128 \pm 1.9$  Ma (MSWD = 4.3) (Fig. 7g). Twenty analyses were conducted on 20 zircons from sample 15QML-83. Among these, spots 16 and 21 were measured on the anhedral gray core domains (Fig. 7h), and they yield older  $^{206}\text{Pb}/^{238}\text{U}$  ages of  $192 \pm 2.0$  and  $381 \pm 8.2$  Ma (Table 2), which might represent the ages of inherited xenocrysts. A group of five relatively old zircons with  $^{206}\text{Pb}/^{238}\text{U}$  ages of  $115 \pm 1.2$  to  $118 \pm 1.3$  Ma (spots 2, 7, 8, 15, and 18) (Table 2) are concordant, forming a tight cluster on the concordia curve (Fig. 7h) with a weighted mean  $^{206}\text{Pb}/^{238}\text{U}$  age of  $117 \pm 1.2$  Ma (MSWD = 4.3),

and these ages may represent crystallization in a magma chamber before the magma ascended to form the pluton in its present position. The other 13 analyses are concordant and yield a weighted mean  $^{206}\text{Pb}/^{238}\text{U}$  age of  $109 \pm 1.1$  Ma (Fig. 7h), and we interpret this as the crystallization age of sample 15QML-83 in the present position of the granitic pluton. Twenty-six analyses of 26 zircons from sample 15QLR-4 are concordant. A group of four very young zircons with  $^{206}\text{Pb}/^{238}\text{U}$  ages of  $31 \pm 0.5$  to  $76 \pm 1.5$  Ma (spots 7, 9, 17, and 23) (Table 2) are possibly related to Cenozoic strike-slip shearing that resulted in metamictization of the zircons and a resetting of the U–Pb system. Three grains yield slightly older  $^{206}\text{Pb}/^{238}\text{U}$  ages of  $129 \pm 2.0$  to  $136 \pm 3.7$  Ma (Fig. 7i), and these data were rejected from the age calculation. The other 19 spots are concordant and yield a weighted mean  $^{206}\text{Pb}/^{238}\text{U}$  age of  $119 \pm 2.1$  Ma (MSWD = 8.2) (Fig. 7i). Twenty-two analyses of 22 zircons from sample 15QLM-37 were conducted. Four discordant zircons (spots 8, 10, 11, and 17) yield  $^{206}\text{Pb}/^{238}\text{U}$  ages of  $111 \pm 1.7$ ,  $128 \pm 3.1$ ,  $132 \pm 1.7$ , and  $137 \pm 1.8$  Ma (Table 2), and were excluded from the age calculation. Eighteen spots are concordant and yield a weighted mean  $^{206}\text{Pb}/^{238}\text{U}$  age of  $122 \pm 2.2$  Ma (MSWD = 8.1) (Fig. 7j). We interpret these weighted mean  $^{206}\text{Pb}/^{238}\text{U}$  ages of  $121 \pm 2.0$ ,  $128 \pm 1.9$ ,  $109 \pm 1.1$ ,  $119 \pm 2.1$ , and  $122 \pm 2.2$  Ma as the crystallization ages of the five granite samples (10QTG-42, 15QML-5, 15QML-83, 15QLR-4, and 15QLM-37, respectively). These ages are consistent with those obtained for the diorites and granodiorites in the Gaoligong Orogen, which suggest all these intrusions were more-or-less coeval and formed in the same tectonic setting.

### 5.3. Zircon Lu–Hf isotopes

Zircons from these eight samples (15QLP-9 and 15QML-5 were not considered) were analyzed for Lu–Hf isotopes on domains with the same or similar structure to those used for U–Pb dating. The results are listed in Table 3. The  $^{176}\text{Lu}/^{177}\text{Hf}$  ratios for all the zircons are less than 0.003, showing a low radiogenetic growth of  $^{176}\text{Hf}$ . The values of  $\varepsilon_{\text{Hf}}^{(t)}$ ,  $T_{\text{DM}}$ , and  $T_{\text{DM}}^{\text{C}}$  were calculated for their respective U–Pb ages.

For gabbroic diorite sample 15QML-65 we performed 17 analyses on 17 zircons. The analytical results show similar Hf isotope compositions, with  $\varepsilon_{\text{Hf}}(t)$  values of +1.2 to +5.4 (Table 3), and the weighted average  $\varepsilon_{\text{Hf}}(t)$  value is  $+3.7 \pm 0.5$  (Fig. 8a), corresponding to single-stage Hf model ages ( $T_{\text{DM}}$ ) of 567–764 Ma and crustal model ages ( $T_{\text{DM}}^{\text{C}}$ ) of 744–979 Ma. The exception was spot 14 which gave a  $\varepsilon_{\text{Hf}}(t)$  value of +10.3 ( $\pm 1.5$ ) and a  $T_{\text{DM}}^{\text{C}}$  age of 467 Ma (Fig. 8b).

With the exception of two spots (15QLL-21-18 and 15QML-57-11) with anomalous  $\varepsilon_{\text{Hf}}(t)$  values of  $+4.4 \pm 3.7$  and  $-1.6 \pm 8.4$ , the zircons from granodiorite samples 15QMH-1, 15QLL-21, and 15QML-57 show negative to positive  $\varepsilon_{\text{Hf}}(t)$  values, ranging from –9.8 to +2.9, and crustal Hf model ages ( $T_{\text{DM}}^{\text{C}}$ ) of 888 to 1564 Ma (Table 3). The weighted average  $\varepsilon_{\text{Hf}}(t)$  value of 56 spots is  $-3.8 \pm 0.7$  (Fig. 8c), corresponding to crustal Hf model ages ( $T_{\text{DM}}^{\text{C}}$ ) of 1000 to 1400 Ma (Fig. 8d).

With the exception of two spots (15QML-83-11 and 15QML-83-17) with anomalous  $\varepsilon_{\text{Hf}}(t)$  values, the zircons from granite samples 10QTG-42, 15QML-83, 15QLR-4, and 15QLM-37 show negative  $\varepsilon_{\text{Hf}}(t)$  values of –8.0 to –1.1 with crustal Hf model ages ( $T_{\text{DM}}^{\text{C}}$ ) of 1101 to 1488 Ma (Table 3). The average  $\varepsilon_{\text{Hf}}(t)$  value for 66 spots is  $-4.4 \pm 0.4$  (Fig. 8e), corresponding to crustal Hf model ages ( $T_{\text{DM}}^{\text{C}}$ ) of 1150 to 1420 Ma (Fig. 8f).

## 6. Discussion

### 6.1. Petrogenesis of the intrusions

#### 6.1.1. Diorites

Lu–Hf zircon data of dated zircons are the most reliable kind of data for tracing the various factors involved in the generation of basic and acid magmas. The  $\varepsilon_{\text{Hf}}(t)$  values of all the concordant zircons from the Early Cretaceous plutons in the Gaoligong Orogen are listed in Table 3.

The gabbroic diorite ( $\delta_2$ ) from our study area displays remarkably restricted initial  $^{176}\text{Hf}/^{177}\text{Hf}$  and  $^{176}\text{Lu}/^{177}\text{Hf}$  values (0.28273–0.28285 and 0.00092–0.00212), and a

narrow range of zircon  $\varepsilon_{\text{Hf}}(t)$  values (+1.2 to +5.4, with a total variation of ca. 4  $\varepsilon_{\text{Hf}}$  units) with Hf crustal model ages ( $T_{\text{DM}}^{\text{C}}$ ) ranging from 744 to 979 Ma except for one anomalous spot (467 Ma) (Table 3). As shown in Fig. 9a, all the data plot in the region between the chondritic Hf evolution (CHUR) and the depleted mantle (DM) lines. This relatively uniform initial Hf isotope signature of the gabbroic diorite reveals the widespread presence of metasomatized subcontinental lithospheric mantle beneath the Gaoligong region, which acted as the source of the mafic magma or as a significant contaminant in asthenospheric mantle magma. These  $\varepsilon_{\text{Hf}}(t)$  values are less than that of recent Atlantic MORB (+8 to +21; Chauvel and Blachert-Toft, 2001). It is possible that primitive mantle-wedge magma was contaminated by minor amounts of crustal material during its migration upwards to a magma chamber.

The contamination of primitive mantle-wedge magma with minor amounts of crustal material is also suggested by the following petrological and geochemical data. (1) The hornblendes in the gabbroic diorite occur as anhedral laths, and some have residual pyroxene cores (Fig. 3a, b), which suggests the amphiboles represent a post-magmatic assemblage that replaced pyroxene crystals at lower temperatures (e.g., Weissman et al., 2013). Furthermore, the dominant mineral assemblage of hornblende with residual pyroxene cores, plagioclase, and K-feldspar shows that this gabbroic diorite is similar to a gabbro. (2) On the diagram of  $\text{SiO}_2$  vs. Mg#, most of the samples plot close to the field of mantle melts and Quaternary basalts (Fig. 10), indicating the gabbro-dioritic magmas are characterized by mantle-derived magmas contaminated by minor amounts of crust-derived material (e.g., Wilson, 1989). The dioritic rocks display linear relationships when plotted on the Th/Yb vs. Ba/La and Th/Yb vs. Sr/Nd diagrams (Fig. 11), and this provides evidence that the initial magmas were enriched in Ba and Sr, which would have come from the slab-derived fluids that enriched the mantle wedge (e.g., Woodhead et al., 2001; Peytcheva et al., 2008; Qi et al., 2016). These data make the metasomatized mantle wedge the best candidate for the primary magma source. (3) Experimental data suggest that calc-alkaline andesites can be generated by the direct partial

melting of hydrous upper mantle at 1.2–2.2 GPa and 1175–1500 °C (e.g., Kushiro, 1974; Parman and Grove, 2004) or by the partial melting of basaltic rocks (e.g., Rapp and Watson, 1995). However, the geochemical characteristics of the gabbroic diorite with its high  $\text{Al}_2\text{O}_3$  (15.21–16.71 wt.%),  $\text{Na}_2\text{O}$  (2.68–2.77 wt.%),  $\text{TiO}_2$  (0.79–1.44 wt.%),  $\text{CaO}$  (9.12–9.61 wt.%), and  $\text{MgO}$  (6.08–7.25 wt.%) contents, Mg# values ranging from 58.1 to 69.5 (Table 1), E-MORB-like chondrite-normalized REE patterns with weak fractionation of LREEs over HREEs, a lack of conspicuous negative Eu anomalies (Fig. 4a), and strongly negative Nb, Ta, and Ti anomalies, show that it was more likely formed from metasomatized mantle melts with partial contributions from crustal materials (e.g., Arevalo and McDonough, 2009; Jiang et al., 2010; Qi et al., 2012, 2016; Sarjoughian et al., 2012; Kananian et al., 2014). The monzodiorite ( $\delta_1$ ), which has variable and sometimes high  $\text{TiO}_2$  and  $\text{K}_2\text{O}$  contents, relatively low  $\text{MgO}$  contents, weak negative Eu and Sr anomalies, and a lack of Nb and Ta anomalies, differs from the gabbroic diorite. On the diagram of  $\text{SiO}_2$  vs. Mg#, all samples fall in the field of basalts (Fig. 10), which indicates the monzodioritic magmas were derived from the partial melting of basaltic rocks. Experimental studies have shown that partial melting of both oceanic and basaltic lower crust can produce dioritic melts (e.g., Castro et al., 2010; Qian and Hermann, 2013). The monzodiorites are characterized by low Sr (280–405 ppm) contents, high Yb (3.2–3.9) contents, and low Sr/Y ratios (8–11) (Table 1), and are notably different from adakitic rocks that form from the partial melting of oceanic crust (e.g., Defant and Drummond, 1990). We consider, therefore, that the monzodiorite was more likely to have been derived from a basaltic lower crust than an oceanic crust, although more isotopic data (Lu–Hf and Sm–Nd) are required to confirm this possibility.

### 6.1.2. Granodiorites and granites

As shown on Fig. 4, the granodioritic and granitic rocks in the Gaoligong Orogen belong to the medium- to high-K calc-alkaline series. Three general processes are

thought to contribute to the origin of calc-alkaline granitoids. (1) Fractional crystallization of mantle-derived magma (which may have been similar in composition to the mafic xenoliths) producing intermediate and felsic magmas (e.g., DePaolo, 1981; Be'eri-Shlevin et al., 2010; Weissman et al., 2013). (2) Melting of crustal rocks by the emplacement of mantle-derived basaltic magmas in the presence of various amounts of water (e.g., Beard and Lofgren, 1989; Weissman et al., 2013). (3) Mixing between mafic and felsic magmas (e.g., DePaolo, 1981; Bergantz, 1989; Roberts and Clemens, 1993; Droop et al., 2003). The dioritic rocks comprise less than 2% of the exposed Early Cretaceous igneous rocks (Fig. 2), they show no cumulate textures, and there are no clear correlations between the major elements and  $\text{SiO}_2$ , Rb and Y, or Sr and Ba, either within the dioritic rocks or between the dioritic and granitic rocks (Fig. 12). Therefore, the first petrogenetic model can be excluded. With the exception of two anomalous spot analyses, the granodiorite samples display a wide range of zircon  $\varepsilon_{\text{Hf}}(t)$  values (−9.8 to +2.9, with a total variation of ca. 13  $\varepsilon_{\text{Hf}}$  units) and  $T_{\text{DM}}^{\text{C}}$  ages of 888 to 1564 Ma, and they plot in a region near the CHUR line in a diagram of  $\varepsilon_{\text{Hf}}(t)$  versus U–Pb age of zircon (Fig. 9a). This indicates a heterogeneous source, possibly produced by the mixing of different proportions of juvenile material and ancient crust (e.g., Kinny and Maas, 2003; Jiang et al., 2009) rather than by the fractional crystallization of mantle-derived basaltic parents or by the partial melting of crustal rocks only. This deduction is consistent with the following lines of evidence. (1) The numerous MMEs in the granodiorite display irregular, ellipsoidal, or round shapes, have transitional zones at their contacts with the host rock, show a halo of felsic leucosome 0.5 to 1 cm wide (Fig. 3c), and have typical igneous textures without cumulate textures (Fig. 3d). In addition, the U–Pb ages of zircons from the MMEs are similar to those of zircons from the host granodiorite (e.g., Zou et al., 2013). These observations indicate that the MMEs are globules of a more mafic magma that was injected into and mingled with the host felsic magma. They are not restites or xenoliths, because restites and xenoliths typically have metamorphic or residual sedimentary fabrics (e.g., White et al., 1999; He et al., 2016; Zhao et al., 2016;

Suzano et al., 2017). (2) The plagioclases (Pl) found as inclusions in K-feldspar (Kf) occur as subhedral to anhedral laths with resorbed borders, and they exhibit a pattern of cores with compositions of An<sub>26–28</sub>, mantles with compositions of An<sub>21–22</sub>, and rims stabilized at An<sub>1–4</sub> together with quartz (Fig. 3e, f). The presence of compositional zoning suggests that the inclusions first grew calcic An-rich cores, and then re-equilibrated at later stages of crystallization after magma mixing, which would indicate they were mechanically transferred from injected mafic magma into the granitic magma (e.g., Suzano et al., 2017). (3) The unique geochemical character of the granodiorites, such as their calc-alkaline and metaluminous characteristics, their high TiO<sub>2</sub>, Na<sub>2</sub>O, and MgO contents, their high values of Mg#, the fact that all samples fall in the region above the field of crustal partial melts on the Mg# vs. SiO<sub>2</sub> diagram (Fig. 10), and the presence of hornblende, reflects the contribution of mantle-derived material in the granodioritic parent magma.

Some of the granites are characterized by their calc-alkaline and peraluminous compositions and the presence of garnet, and they are considered to be S-types derived by the melting of metasedimentary crust (e.g., Chappell et al., 1987), but the other granites are calc-alkaline and metaluminous, and considered to be I-types derived by the melting of meta-igneous rocks or by the mixing of mafic and felsic magmas (e.g., Clemens et al., 2011; Weissman et al., 2013; Oliveira et al., 2015; Wang et al., 2015). As shown in Fig. 8, all the zircons from our granitic samples, except for two anomalous spot analyses, show negative  $\varepsilon_{\text{Hf}}(t)$  values (−8.0 to −1.1, with an average at −4.4) and  $T_{\text{DM}}^{\text{C}}$  values of 1101 to 1488 Ma, and they fall in the region below the line of CHUR, suggesting an ancient crustal source (Fig. 9). However, the large scatter in  $\varepsilon_{\text{Hf}}(t)$  values, and the fact they plot close to the line of CHUR, suggests the magmas originated mainly from a crustal source that was contaminated with small amounts of mantle-derived components (rather than from meta-igneous rocks), and they might reflect lesser degrees of homogenization of the crust-derived magma after mixing with the mantle-derived magma (e.g., Peytcheva et al., 2008; Jiang et al., 2009; Zhu et al., 2009; Shellnutt et al., 2011). Furthermore, the granites have a wide range of Mg# values (35.9–51.3) and Sr

contents (91–207 ppm) that are mostly higher than those found in pure crustal partial melts (Fig. 10). Moreover, there is no clear correlation between Ba and Sr or Rb and Y (Fig. 12), and in the study area, significant contributions of mantle-derived magma are recorded in the dioritic group by the positive  $\varepsilon_{\text{Hf}}(t)$  values. To reveal the initial magma evolutionary paths of these granitoids, application of rhyolite-MELTS (e.g., Gualda et al., 2012; Gardner et al., 2014), using compositions that vary from granodiorite to granite, shows that: 1) the granodioritic magma derived from the lower crust (LC), and the concentrations of SiO<sub>2</sub> increase with increasing pressure from 0.8 to 2.0Gpa (Fig. 13a-c). Obviously, it is not in accordance with the depth of crust in continental margin, and the magnesian features (e.g., Huang and He, 2010; Murphy et al., 2018); 2) the granitic magma derived from the partial melting of the middle to upper crust, the SiO<sub>2</sub> contents and K<sub>2</sub>O/Na<sub>2</sub>O ratios increase with decreasing pressure, but they are not exactly consistent with the pressure curve also (Fig. 13a-c). On the other hand, it probably indicates that the sampled rocks are not pure the crust-derived compositions but rather represent mixtures of crust- and mantle- derived magmas. The binary mixing modeling based on the major oxides, trace elements and radiogenic isotope signatures had been used to show the degrees of mixing of mafic and felsic melts (e.g., Langmuir et al., 1978; Patino-Douce, 1999; Rudnick and Gao, 2003; Healy et al., 2004; Wang et al, 2015; Ghaffari et al., 2015; Stouraiti et al., 2018). In the Na<sub>2</sub>O/CaO vs. MgO/Al<sub>2</sub>O<sub>3</sub> diagram (Fig.13d), the data plots with the plutonic compositions close to the binary mixing curve, show that the hybrid of magma of the diorite, granodiorite and granite were generated by 65 to 85%, 10 to 25 % and 5 to 15 % mafic melts, and 15 to 35%, 65 to 75 and 85 to 95 felsic melts, respectively. We infer, therefore, that the granodioritic and granitic magmas originated mainly from the partial melting of ancient upper crustal materials, and these melts were mixed with variable amounts of mantle-derived magma.

## 6.2. Tectonic setting

The Early Cretaceous magmatic rocks in the Gaoligong Orogen are dominantly I-type, and composed mainly of diorite, granodiorite, and granite. Even though the geochemical characteristics of the magmatic rocks, such as their metaluminous and calc-alkaline compositions, their enrichment in LILEs (Th, U, Ba, K, and Rb) and LREEs, and their strong negative Nb, Ta, P, and Ti anomalies (Fig. 5d, f), are typical of calc-alkaline magmatism, this magmatism could possibly have been generated in subduction, syn-collisional, or post-collisional tectonic settings. Peraluminous granites traditionally considered to be formed in collision-related setting rather than subduction-related and rift setting (e.g., Pearce et al., 1984; Sylvester, 1998; Barbarin, 1999, Xu et al., 2012). The magmatic rocks derived from the crustal melting and mixing by influx of mantle-derived magma are common in subduction-related setting, but rare intracrustal setting (e.g., Xu et al., 2012). The Early Cretaceous magmatic rocks in the Gaoligong Orogen form a belt or linear distribution, and this precludes the possibility of post-collisional magmatism throughout such a large region. The assemblage of diorite, granodiorite, and granite, characterized by a wide range in  $\text{SiO}_2$  content (50.95 to 76.49%), and  $\varepsilon_{\text{Hf}}(t)$  values (-9.8 to +5.4), high  $\text{Mg}^{\#}$ , magnesian affinity and absence of muscovite-bearing leucogranite and syenogranite also excludes the possibility of a syn-collisional setting (e.g., Harris et al., 1990; Harrison et al., 1998; Frost et al., 2001). Furthermore, as mentioned earlier, the dioritic magmas were derived from melts of metasomatized mantle, with the melts contaminated with small amounts of crustal material, and the granodioritic and granitic magmas originated mainly from the partial melting of ancient upper crustal materials, with the melts mixed with variable amounts of mantle-derived magma. In other words, there was a significant contribution of mantle-derived material to the magmas, and the magmatism was related to subduction rather than collision. We propose, therefore, that these calc-alkaline magmatic rocks were generated in a subduction-related tectonic setting (e.g., Kelemen et al., 1990; Stolz et al., 1996; Barbarin, 1999; Sheth et al., 2002; Castillo et al., 2007; Munteanu and Wilson, 2009; Dong et al., 2012; Qi et al., 2012, 2014, 2016; Ashwal et al., 2013; Sreejith and Ravindra, 2013; Collins et al.,

2016). This finding is supported by tectonic discrimination diagrams, as for example in the Hf– $^{3*}$ Ta–Rb/30 and Rb vs. Y + Nb tectonic discrimination diagrams (Fig. 14a, b), where all the granitoid samples fall within the field of volcanic arc (and syn-collisional) granites. This is also demonstrated by the Al<sub>2</sub>O<sub>3</sub>–MgO–FeO<sub>t</sub> and La/Yb vs. Th/Yb tectonic discrimination diagrams, where all the dioritic samples fall within the continental margin-arc or island arc fields (Fig. 14c, d), and where the granitic samples fall in the continental margin-arc field (Fig. 14d). In addition, the strata in the BNS and the Gaoligong Orogen were deposited under marine conditions until at least ~118 Ma (even until 115–100 Ma), and the Upper Cretaceous nonmarine clastic sediments with basal conglomerates (75–90 Ma) in the Baingoin area unconformably overlie Early Cretaceous marine sediments (e.g., Yunnan Bureau Geological Mineral Resource, 1991; Kapp et al., 2005, 2007; Chen et al., 2017; Zhu et al., 2017), indicating that the subducted Bangong – Nujiang oceanic slab was still active between the Tengchong – Lhasa and Baoshan–Qiangtang blocks until at least ~118 Ma. The mélange belt along the southeastern margin of the Gaoligong Orogen (Fig. 2) is mainly composed of abyssal facies flysch sedimentary rocks with siliceous rock (Upper Triassic to Jurassic) and slices of serpentine peridotite, basalt, gabbro / diabase. The serpentine peridotite contains dunite and harzburgite ( $F_o=89\text{--}92$ ), chromite ( $\text{Cr}^{\#}=72\text{--}88$ ,  $\text{Mg}^{\#}=19\text{--}39$ ). The SiO<sub>2</sub>, Al<sub>2</sub>O<sub>3</sub> and FeO<sub>t</sub> contents vary from 39.66 to 40.97 wt.%, 0.34 to 0.42 wt.% and 7.45 to 9.33 wt.% (unpublished), respectively. This features resembles the Upper Triassic to Jurassic ophiolitic mélange belt in the BNS (e.g., Tan and Zhan, 1990; Liu et al., 2002; Yin et al., 2012), and it gives clear evidence for a subduction-related setting. Furthermore, besides I-type granites, there are some S-type granites in Gaoligong Orogen, with high Sr isotopic ratios and negative  $\varepsilon_{\text{Nd}}$  and  $\varepsilon_{\text{Hf}}(t)$  values (-2 to -12), showing a significantly crustal sources (e.g., Xu et al., 2012). It is reasonable, therefore, to conclude that all these plutons, including the diorites, granodiorites, and granites, were generated along an active continental margin within a subduction-related tectonic setting during the transformation of subduction into collision. The fluids released from the subducted

slab and overlying sediments as a result of multistage dehydration would have migrated upwards through the overlying mantle wedge, resulting in metasomatism and melting of the wedge (e.g., Iwamori, 1998, 2007; Nakamura and Iwamori, 2009; Zhu et al., 2010; Qi et al., 2014). The mantle-derived magma was injected into the overlying crust, resulting in the partial melting of crustal rocks to produce granitic magma. The mafic magmas mixed with the crustal melts in different proportions to produce various dioritic and granitoid magmas (Fig. 15). The mélange was formed due to the tectonic mixing of materials from the oceanic and continental crusts.

### 6.3. Connection of the Gaoligong and Bangonghu–Nujiang sutures

The Early Cretaceous intermediate to acidic magmatic belt of the Gaoligong Orogen runs southwards towards the Mogok belt in Myanmar (e.g., Chen et al., 2016) and northwards towards Bomi–Chayu in Tibet (e.g., Chiu et al., 2009; Zhu et al., 2009) and towards the BNS that marks the boundary between the Lhasa and Qiangtang blocks (e.g., Zhu et al., 2011, 2015; Xu et al., 2012; Zhang et al., 2017). A comparison of the Early Cretaceous magmatic rocks of Bomi–Chayu and the BNS with those from the Gaoligong Orogen shows that they share many similarities in rock assemblages, emplacement ages, major and trace elemental compositions, and isotopic data (Fig. 9), indicating that the Early Cretaceous magmatic belt in the Gaoligong Orogen was linked with that in Bomi–Chayu and the BNS. More importantly, the ophiolitic mélange belt, the Middle Jurassic basaltic magmatism, and the marine-facies paleontological and stratigraphic features of the Gaoligong Orogen are very similar to features in the BNS (e.g., Tibet Geological Survey Institute, 2001; Yunnan Geological Survey Institute, 2011) (Fig. 2). This resemblance implies that the Gaoligong Orogen and BNS had similar tectonomagmatic histories in the Mesozoic. Furthermore, the following lines of evidence show that the Tengchong Block should be linked with the Lhasa Block. (1) The Tengchong Block records magmatic activity in the Cambrian–Ordovician, Triassic, Early Cretaceous, Late Cretaceous, and Paleocene–Eocene, and the

spatial and temporal distributions of these magmatic rocks, as well as their petrological and geochemical features, closely resemble those in the Lhasa Block, but differ significantly from those in the Baoshan and Western Qiangtang blocks (e.g., Zhu et al., 2009, 2011; Qi et al., 2011, 2015; Xu et al., 2012; Xie et al., 2016; Zhao et al., 2016). (2) Liao et al. (2015) preferred the idea that the Tengchong Block was an individual tectonic unit located to the northeast of the Lhasa Block between the Sibumasu Block and northern Australian Gondwana, rather than it being part of the Sibumasu Block, since the Tengchong Block shares similar Permian paleontological and stratigraphic features to the Lhasa Block. (3) Latest study has suggested that the significant Nankinella-Chusenella fusuline assemblage occurs in the Lhasa and Tengchong Blocks, and lacks in either the South Qiangtang Block or the Gondwanan margin, indicating that the Lhasa and Tengchong blocks were isolated from both the South Qiangtang Block and the northern Gondwanan margin during the Middle Permian (e.g., Zhang et al., 2018). In addition, Early Permian plume-derived basalts are absent in the Lhasa and Tengchong blocks, which illustrates the considerable differences between these two blocks and the Sibumasu Block (e.g., Wopfner, 1996; Shi et al., 2008; Zhang et al., 2013; Liao et al., 2015). We argue, therefore, that the Tengchong Block should be linked with the Lhasa Block and that the Gaoligong Orogen represents the suture between the Tengchong and Baoshan blocks, and that it is the southward extension of the BNS around the Eastern Himalayan Syntaxis.

## 7. Conclusions

The dioritic, granodioritic, and granitic rocks in the Gaoligong Orogen, south of the Eastern Himalayan Syntaxis, belong to the medium- to high-K calc-alkaline series. LA–ICP–MS U–Pb dating of the zircons from these rocks reveal Early Cretaceous emplacement ages (128–109 Ma).

Zircons from the dioritic rocks have  $\epsilon_{\text{Hf}}(t)$  values of +1.2 to +5.4 with  $T_{\text{DM}}^{\text{C}}$  ages of

744 to 979 Ma, those from the granodiorites have  $\varepsilon_{\text{Hf}}(t)$  values of -9.8 to +2.9 with  $T_{\text{DM}}^{\text{C}}$  ages of 888 to 1564 Ma, while those from the granites have  $\varepsilon_{\text{Hf}}(t)$  values of -8.0 to -1.1 with  $T_{\text{DM}}^{\text{C}}$  ages of 1101 to 1488 Ma. The hornblendes in the dioritic rocks contain residual pyroxene cores, and the granodiorites contain mafic microgranular enclaves (MMEs). In combination with their general geochemical characteristics and their locations on tectonic discrimination diagrams, these features suggest that the dioritic and granitic magmas were produced by the mixing of variable proportions of mantle- and crust-derived magmas along an active continental margin within a subduction-related (continental-arc) tectonic setting.

The ages and tectonic settings of the intermediate and felsic rocks are similar to those of rocks in the Bangong–Nujiang Suture (BNS) to the north of the Lhasa Block, and to the north of the Eastern Himalayan Syntaxis, indicating a similar history and a synchronous episode of crustal growth/recycling during the Early Cretaceous. The Tengchong Block in SW Yunnan (south of the Eastern Himalayan Syntaxis) has early Permian paleontological and stratigraphic features in common with the Lhasa Block, but these features differ from those of the Sibumasu Block, which implies that the Tengchong Block was linked to the Lhasa Block rather than the Sibumasu Block. The evidence therefore leads us to propose that the Gaoligong Orogen represents the suture between the Tengchong and Baoshan blocks, and that it is the southward extension of the BNS around the Eastern Himalayan Syntaxis.

### Acknowledgements

We would like to thank Prof. Shellnutt, J.G. and Xiao, W.J. for their comments, Prof. Zhang, Z.M., Zeng, L.S. and Luo, Z.H. for their discussion and help, and Stallard Scientific Editing for its linguistic assistance during the preparation of this manuscript. This study was supported by NSFC project (91755101, 41272219), the Chinese Ministry of Science and Technology (Sinoprobe-05-03) and the China Geological Survey (1212011020000150005-07).

## References

- Ali, J.R., Cheung, H.M.C., Aitchison, J.A., Sun, Y.D., 2013. Palaeomagnetic re-investigation of Early Permian rift basalts from the Baoshan Block, SW China: constraints on the site of origin of the Gondwana-derived eastern Cimmerian terranes. *Geophysical Journal International* 193, 650-663.
- Arculus, R.J., 2003. Use and abuse of the terms calcalkaline and calcalkalic. *Journal of Petrology* 44, 929-935.
- Arevalo, R., McDonough, W. F., 2009. Global MORB = N-MORB + E-MORB. *American Geophysical Union, Fall Meeting 2009*. AGU.
- Ashwal, L.D., Solanki, A.M., Pandit, M.K., Corfu, F., Hendriks, B.W.H., Burke, K., Torsvik, T.H., 2013. Geochronology and geochemistry of Neoproterozoic Mt. Abu granitoids, NW India: Regional correlation and implications for Rodinia paleogeography. *Precambrian Research* 236, 265-281.
- Barbarin, B., 1999. A review of the relationships between granitoid types, their origins and their geodynamic environments. *Lithos* 46, 605-626.
- Beard, J.B., Lofgren, G.E., 1989. Effect of water on the composition of partial melts of greenstone and amphibolites. *Science Magazine* 244, 195-197.
- Be'eri-Shlevin, Y., Katzir, Y., Blichert-Toft, J., Kleinhanns, I.C., Whitehouse, M., 2010. Nd-Sr-Hf-O isotope provinciality in the northernmost Arabian-Nubian Shield: Implications for crustal evolution. *Contributions to Mineralogy and Petrology* 160, 181-201.
- Bergantz, G.W., 1989. Underplating and partial melting: Implications for melt generation and extraction. *Science* 245, 1093-1095.
- Blichert-Toft, J., Albarède F., 1997. The Lu-Hf geochemistry of chondrites and the evolution of the mantle-crust system. *Earth and Planetary Science Letters* 148, 243-258.
- Büchl, A., Brugmann, G., Batanova, V.G., 2004. Formation of podiform chromitite deposits: Implications from PGE abundances and Os isotopic compositions of chromites from the Troodos complex, Cyprus. *Chemical Geology* 208, 217-232.

- Cai, Z.H., Xu, Z.Q., Duan, X.D., Li, H.Q., Gao, H., Huang, X.M., 2013. Early stage of Early Paleozoic orogenic event in western Yunnan Province, southeastern margin of Tibet Plateau. *Acta Petrologica Sinica* 29 (6), 2123 – 2140 (in Chinese with English abstract).
- Castillo, P.R., Rigby, S.J., Solidum, R.U., 2007. Origin of high field strength element enrichment in volcanic arcs: Geochemical evidence from the Sulu Arc, southern Philippines. *Lithos* 97, 271-288.
- Castro, A., Gerya, T., Garcia-Casco, A., Fernandez, C., Diaz-Alvarado, J., Moreno-Ventas, I., Low, I., 2010. Melting relations of MORB-sediment mélange in underplated mantle wedge plumes: implications for the origin of cordilleran-type batholiths. *Journal of Petrology* 51:1267–1295.
- Chauvel, C. and Blichert-Toft, J., 2001. A hafnium isotope and trace element perspective on melting of the depleted mantle. *Earth and Planetary Science Letters*, 190, 137-151.
- Chappell, B., White, A., Wyborn, D., 1987. The importance of residual source material (restite) in granite petrogenesis. *Journal of Petrology* 28, 1111-1138.
- Chauvel, C. and Blichert-Toft, J., 2001. A hafnium isotope and trace element perspective on melting of the depleted mantle. *Earth and Planetary Science Letters* 190, 137-151.
- Chen, S.S., Shi, R.D., Gong, X.H., Liu, D.L., Huang, Q.S., Yi, G.D., Wu, K., Zou, H.B., 2017., A syn-collisional model for Early Cretaceous magmatism in the northern and central Lhasa subterranea. *Gondwana Research* 41 (2017) 93–109.
- Chen, X.J., Xu, Z.Q., Sein, K., Meng, Y.K., Cai, Z.H., 2016. The early Cretaceous tectonic magmatism in the Mogok district, central Myanmar, and its implication for the evolution of Tethys. *Acta Geologica sinica* 90, 3060-3080 (in Chinese with English abstract).
- Chiu, H.Y., Chung, S.L., Wu, F.Y., Liu, D.Y., Liang, Y.H., Lin, I.J., Iizuka, Y., Xie, L.W., Wang, Y.B., Chu, M.F., 2009. Zircon U-Pb and Hf isotope constraints from eastern Transhimalayan batholiths on the precollisional magmatic and tectonic evolution in southern Tibet. *Tectonophysics* 477, 3-19.
- Chu, Z.Y., Wang, W., Chen, F.K., Wang, X.L., Li, X.H., Ji, J.Q., 2009. Os-Nd-Pb-Sr isotopic compositions of the Santaishan ultramafic rock in western Yunnan and its geological significances. *Acta Petrologica Sinica* 25, 3221-3228 (in Chinese with English abstract).

- Clemens, J.D., Stevens, G., Farina, F., 2011. The enigmatic sources of I-type granites: The peritectic connexion. *Lithos* 126, 174-181.
- Collins, W.J., Huang, H.Q., Jiang X.Y., 2016. Water-fluxed crustal melting produces Cordilleran batholiths. *Geology* doi:10.1130/G37398.1
- Cong, F., Lin, S.L., Zou, G.F., Li, Z.H., Xie, T., Peng, Z.M., Liang, T., 2011. Magma mixing of granites at Lianghe: In-situ zircon analysis for trace elements, U-Pb ages and Hf isotopes. *Science China: Earth Sciences* 54, 1346–1359.
- Coulon, C., Maluski, H., Bollinger, C., Wang, S., 1986. Mesozoic and Cenozoic volcanic rocks from central and southern Tibet:  $^{39}\text{Ar}$ - $^{40}\text{Ar}$  dating, petrological characteristics and geodynamical significance. *Earth and Planetary Science Letters* 79, 281-302.
- Defant, M.J., Drummond, M.S., 1990. Derivation of some modern arc magmas by melting of young subducted lithosphere. *Nature* 347 (6294), 662–665.
- DePaolo, D.J., 1981. A neodymium and strontium isotopic study of the Mesozoic calc-alkaline granitic batholiths of the Sierra Nevada and Peninsular Ranges, California. *Journal of Geophysical Research* 86, 10470–10488.
- Dong, Y.P., Liu, X.M., Zhang, G.W., Chen, Q., Zhang, X.N., Li, W., Yang, C., 2012. Triassic diorites and granitoids in the Foping area: Constraints on the conversion from subduction to collision in the Qinling orogen, China. *Journal of Asian Earth Sciences* 47, 123-142.
- Droop, G.T.R., Clemens, J.D., Dalrymple, D.J., 2003. Processes and conditions during contact anatexis, melt escape and restite formation: The Hunly Gabbro complex, NE Scotland. *Journal of Petrology* 44, 995-1029.
- Eroğlu, S., Siebel,W., Danišík, M., Pfänder, J.A., Chen, F.K., 2013. Multi-system geochronological and isotopic constraints on age and evolution of the Gaoligongshan metamorphic belt and shear zone system in western Yunnan, China. *Journal of Asian Earth Sciences* 73, 218-239.
- Fan, J.J., Li, C., Xie, C.M., Wang, M., Chen, J.W., 2015. The evolution of the Bangong–Nujiang Neo-Tethys ocean: Evidence from zircon U–Pb and Lu–Hf isotopic analyses of Early Cretaceous oceanic islands and ophiolites. *Tectonophysics* 655, 27-40.
- Frost, B.R., Brans, C.G., Collins, W.J., Arculus, R.J., Ellis, D.J., Frost, C.D., 2001. Geochemical classification for granitic rocks. *Journal of Petrology* 42, 2033-2048.

- Gardner, J.E., Befus, K.S., Gualda, G.A.R., Ghiorso, M.S., 2014. Experimental constraints on rhyolite-MELTS and the Late Bishop Tuff magma body. Contributions to Mineralogy and Petrology 168, 1051-1065.
- Ghaffari, M., Rashidnejad-Omrani, N., Dabiri, R., Santos, J.F., Mata, J., Buchs, D., McDonald, I., Appel, P., Garbe-Schoenberg, D., 2015. Interaction between felsic and mafic magmas in the Salmas intrusive complex, Northwestern Iran: Constraints from petrography and geochemistry. Journal of Asian Earth Sciences 111, 440-458.
- Gualda, G.A.R., Ghiorso, M.S., Lemons R.V., Carley T.L., 2012. Rhyolite-MELTS: A modified calibration of MELTS optimized for silica-rich, fluid-bearing magmatic systems. Journal of Petrology 53, 875-890.
- Guynn, J.H., Kapp, P., Pullen, A., Gehrels, G., Heizler, M., Ding, L., 2006. Tibetan basement rocks near Amdo reveal “missing” Mesozoic tectonism along the Bangong suture, central Tibet. Geology 34, 505-508.
- Harris, N.B.W., Pearce, J.C., Tindle, A.G., 1986. Geochemical characteristics of collision-zone magmatism. In: Coward, M.P. and Reis, A.C. (eds.), Collision tectonics. Special Publication Geological Society 19, 67-81.
- Harris, N.B.W., Inger, S., Ronghua, X., 1990. Cretaceous plutonism in Central Tibet: An example of post-collision magmatism? Journal of Volcanology and Geothermal Research 44, 21-32.
- Harrison, T.M., Grove, M., Lovera, O.M., Catlos, E.J., 1998. A model for the origin of Himalayan anatexis and inverted metamorphism. Journal of Geophysical Research 103, 27017–27032.
- He, W.Y., Mo, X.X., Yang, L.Q., Xing, Y.L., Dong, G.C., Yang, Z., Gao, X., Bao, X.S., 2016. Origin of the Eocene porphyries and mafic microgranular enclaves from the Beiya porphyry Au polymetallic deposit, western Yunnan, China: Implications for magma mixing/mingling and mineralization. Gondwana Research 40, 230-248.
- Healy, B., Collins, W.J., Richards, S.W., 2004. A hybrid origin for Lachlan S-type granites: The Murrumbidgee Batholith example. Lithos 78, 197- 216.
- Hoskin, P.W.O., Schaltegger, U., 2003. The composition of zircon and igneous and metamorphic petrogenesis. In: Zircon. Hanchar, J. M., Hoskin, P.W.O., eds., Reviews in Mineralogy and Geochemistry 53, 27-55.

- Hsü, K.J., Pan, G.T., Sengör, A.M.C., 1995. Tectonic evolution of the Tibetan Plateau: A working hypothesis based on the archipelago model of orogenesis. International Geology Review 37, 473-508.
- Hu, Z.C., Liu, Y.S., Gao, S., Liu, W.G., Yang, L., Wen Zhang, W., Tong, X.R., Lin, L., Zong, K.Q., Li, M., Haihong Chen, H.H., Zhou, L., 2012. Improved in situ Hf isotope ratio analysis of zircon using newly designed X skimmer cone and Jet sample cone in combination with the addition of nitrogen by laser ablation multiple collector ICP-MS, Journal of Analytical Atomic Spectrometry 27, 1391-1399.
- Huang F. and He Y.S., 2010. Partial melting of the dry mafic continental crust: Implications for petrogenesis of C-type adakites. Chinese Science Bulletin 55, 2428-2439.
- Iwamori, H., 1998. Transportation of H<sub>2</sub>O and melting in subduction zones. Earth and Planetary Science Letters 160, 65-80.
- Iwamori, H., Richardson, C., Maruyama, S., 2007. Numerical modeling of thermal structure, circulation of H<sub>2</sub>O, and magmatism–metamorphism in subduction zones: Implications for evolution of arcs. Gondwana Research 11, 109-119.
- Ji, W.Q., Wu, F.Y., Chung, S.L., Li, J.X., Liu, C.Z., 2009. Zircon U–Pb chronology and Hf isotopic constraints on the petrogenesis of Gangdese batholiths, southern Tibet. Chemical Geology 262, 229-245.
- Jiang, Y.H., Jiang, S.Y., Dai, B.Z., Liao, S.Y., Zhao, K.D., Ling, H.F., 2009. Middle to Late Jurassic felsic and mafic magmatism in southern Hunan Province, Southeast China: Implications for a continental arc to rifting. Lithos 107, 185-204.
- Jiang, Y. H., Jin, G., D., Liao, S., Y., Zhou, Q., Zhao, P., 2010. Geochemical and Sr–Nd–Hf isotopic constraints on the origin of Late Triassic granitoids from the Qinling orogen, central China: Implications for a continental arc to continent–continent collision. Lithos 117, 183-197.
- Kananian, A., Sarjoughian, F., Nadimi, A., Ahmadian, J., Wenli Ling, W.L., 2014. Geochemical characteristics of the Kuh-e Dom intrusion, Urumieh–Dokhtar Magmatic Arc (Iran): Implications for source regions and magmatic evolution. Journal of Asian Earth Sciences 90, 137-148.
- Kapp, P., Murphy, M.A., Yin, A., Harrison, T.M., Ding, L., Guo, J.R., 2003. Mesozoic and Cenozoic tectonic evolution of the Shiquanhe area of western Tibet. Tectonics 22, 1029.

- Kapp, P., Yin, A., Harrison, T.M., Ding, L., 2005. Cretaceous–Tertiary shortening, basin development, and volcanism in central Tibet. Geological Society of America Bulletin 117, 865–878.
- Kapp, P., DeCelles, P.G., Gehrels, G.E., Heizler, M., Ding, L., 2007. Geological records of the Lhasa–Qiangtang and Indo-Asian collisions in the Nima area of central Tibet. GSA Bulletin 119, 917–932.
- Kelemen, P.B., Kingler, R.J., Johnson, K.T.M., 1990. High field strength element depletions in arc basalts due to mantle-magma interaction. Nature 345, 521–524.
- Kinny, P.D., Maas, R., 2003. Lu–Hf and Sm–Nd isotope systems in zircon. In: Hanchar, J.M., Hoskin, P.W.O. (Eds.), Zircon. Reviews in Mineralogy and Geochemistry 53, 327–341.
- Kushiro, I., 1974. Melting of hydrous upper mantle and possible generation of andesitic magma: An approach from synthetic systems. Earth and Planetary Science Letters 22, 294–299.
- Langmuir, C.H., Robert D. Vocke Jr, R.D., Hanson, G.N., Hart, S. R., 1978. A general mixing equation with applications to Icelandic basalts. Earth and Planetary Science Letters, 37, 380–392.
- Le Maitre, R.W., Bateman, P., Dudek, A., Keller, J., Lameyre Le Bas M.,J., Sabine, P.A., Schmid, R., Sorensen, H., Streckeisen, A., Woolley, A.R., Zanettin, B., 1989. A classification of igneous rocks and glossary of terms. Blackwell, Oxford.
- Li, Z.H., Lin, S.L., Cong, F., Zou, G.F., 2012. U-Pb ages of zircon from metamorphic rocks of the Gaoligongshan Group in western Yunnan and its tectonic significance. Acta Petrologica Sinica 28 (5), 1529–1541 (in Chinese with English abstract).
- Liao, S.Y., Wang, D.B., Tang, Y., Yin, F.G., Cao, S.N., Wang, L.Q., Sun, Z.M., 2015. Late Paleozoic Woniusi Basaltic Province from Sibumasu terrane: Implications for the break-up of eastern Gondwana's northern margin. Geological Society of America Bulletin 127 (9-10), 1313–1330.
- Liu, B.P., Feng, Q.L., Chonglakmani, C., Helmcke, D., 2002. Framework of Paleotethyan Archipelago Ocean of western Yunnan and its elongation towards north and south. Earth Science Frontiers 9 (3), 161–171 (in Chinese with English abstract).
- Liu, C.Z., Wu, F.Y., Chu, Z.Y., Ji, w.Q., Yu., L.J., Li, J.L., 2012. Preservation of ancient Os isotope signatures in the Yungbwa ophiolite (southwestern Tibet) after subduction

- modification. *Journal of Asian Earth Sciences* 53, 38–50.
- Liu, C.Z., Chung, S.L., Wu, F.Y., Zhang, C., Xu., Y., wang, J.G., Chen, Y., Guo., S., 2016. Tethyan suturing in Southeast Asia: Zircon U-Pb and Hf-O isotopic constraints from Myanmar ophiolites. *Geology* 44, 311-314.
- Liu, J.L., Song, Z.J., Cao, S.Y., Zai, Y.F., Wang, A.J., Gao, L., Xiu, Q.Y., Cao, D.H., 2006. The dynamic setting and processes of tectonic and magmatic evolution of the oblique collision zone between Indian and Eurasian plates: Exemplified by the tectonic evolution of the Three River region, eastern Tibet. *Acta Petrologica Sinica* 22, 775-786 (in Chinese with English abstract).
- Lopez-Escobar, L., Kilian, R., Kempton, P., Tagiri, M., 1993. Petrography and geochemistry of Quaternary rocks from the Southern Volcanic Zone of the Andes between 41°30' and 46°00'S, Chile. *Andean Geology* 20, 33-55.
- Ma, L.Y., Wang, Y.J., Fan, W.M., Geng, H.Y., Cai, Y.F., Zhong, H., Liu, H.C., Xing, X.W., 2014. Petrogenesis of the early Eocene I-type granites in west Yingjiang (SW Yunnan) and its implication for the eastern extension of the Gangdese batholiths. *Gondwana Research* 25, 401-419.
- Martin CE. 1994. Osmium isotopic characteristics of mantle-derived rocks. *Geochem. Cosmochim. Acta* 55, 1421-1434.
- Metcalfe, I., 2002. Permian tectonic framework and palaeogeography of SE Asia. *Journal of Asian Earth Sciences* 20, 551-566.
- Metcalfe, I., 2013. Gondwana dispersion and Asian accretion: Tectonic and palaeogeographic evolution of eastern Tethys. *Journal of Asian Earth Sciences* 66, 1-33.
- Metcalfe, I., Aung, K.P., 2014. Late Tournaisian conodonts from the Taungnyo Group near Loi Kaw, Myanmar (Burma): Implications for Shan Plateau stratigraphy and evolution of the Gondwana-derived Sibumasu Terrane. *Gondwana Research* 26, 1159-1172.
- Mitchell, A.H.G., 1993, Cretaceous–Cenozoic tectonic events in the western Myanmar (Burma)-Assam region. *Journal of the Geological Society* 150, 1089-1102.
- Munteanu, M., Wilson, A., 2009. The South China piece in the Rodinian puzzle. A comment on “Assembly, configuration, and break-up history of Rodinia: A synthesis by Li et al. (2008) [Precambrian Res. 160, 179e210]. *Precambrian Research* 171, 74-76.

- Murphy, J.B., Shellnutt, J.G., Collins, W., 2018. Late Neoproterozoic to Carboniferous genesis of A-type magmas in the Avalonian Terrane of northern Nova Scotia: Repeated partial melting of anhydrous lower crust in contrasting tectonic environments. International Journal of Earth Sciences 107, 587-599.
- Nakamura, H. and Iwamori, H., 2009. Contribution of slab-fluid in arc magmas beneath the Japan arcs. Gondwana Research 16, 431-445.
- Oliveira, E.P., Bueno, J.F., McNaughton, N.J., Filho, A.F.S., Nascimento, R.S., Donatti-Filho, J., 2015. Age, composition, and source of continental arc- and syn- collision granites of the Neoproterozoic Sergipano Belt, Southern Borborema Province, Brazil. Journal of South American Earth Sciences 58, 257-280.
- Pan, G.T., Mo, X.X., Hou, Z.Q., Zhu, D.C., Wang, L.Q., Li, G.M., Zhao, Z.D., Geng, Q.R., Liao, Z.L., 2006. Spatial-temporal framework of the Gangdese Orogenic Belt and its evolution. Acta Petrologica Sinica 22, 521-533 (in Chinese with English abstract).
- Parman, S.W., Grove, T.L., 2004. Harzburgitemelting with and without  $H_2O$ : Experimental data and predictive modeling. Journal of Geophysical Research 109 (B02201), 1-20.
- Patino-Douce, A.E., 1999. What do experiments tell us about the relative contributions of crust and mantle to the origin of granitic magmas? In: Castro, A., Fernandez, C., Vigneresse, J.L. (Eds.), Understanding Granites: Integrating New and Classical Techniques. Geological Society Special Publications, 168, 55-75.
- Pearce, J.A., Gale, G.H., 1977. Identification of ore-deposition envoriment from trace element geochemistry of associated igneous host rocks. Geological Society London Special Publication 7, 14-24.
- Pearce, J.A., Harris, B.W., Tindle, A.G., 1984. Trace element discrimination diagrams for the tectonic interpretation of granitic rocks. Journal of Petrology 4, 956-983.
- Peccerillo, R. and Taylor, S.R., 1976. Geochemistry of Eocene calc-alkaline volcanic rocks from the Kastamonu area, northern Turkey. Contributions to Mineralogy and Petrology 58, 63-81.
- Peytcheva, I., Quadt, A.V., Georgiev, N., Ivanov, Z., Heinrich, C.A., M. Frank, M., 2008. Combining trace-element compositions, U-Pb geochronology and Hf isotopes in zircons to unravel complex calcalkaline magma chambers in the Upper Cretaceous Srednogorie zone (Bulgaria). Lithos 104, 405-427.

- Qi, X.X., Zhu, L.Z., Hu, Z.C., Li, Z.Q., 2011. Zircon SHRIMP U–Pb dating and Lu–Hf isotopic composition for Early Cretaceous plutonic rocks in Tengchong block, southeastern Tibet, and its tectonic implications. *Acta Petrologica Sinica* 27 (11), 3409–3421 (in Chinese with English abstract).
- Qi, X.X., Zeng, L.S., Zhu, L.H., Hu, Z.C., Hou K.J., 2012. Zircon U-Pb and Lu-Hf isotopic systematics on the Daping plutonic rocks: Implications for the Neoproterozoic tectonic evolution in the northeastern margin of the Indochina block, Southwest China. *Gondwana Research* 21, 180-193.
- Qi, X.X., Santosh, M., Zhu, L.H., Zhao, Y.H., Hu, Z.C., Zhang, C., Ji, F.B., 2014. Mid-Neoproterozoic arc magmatism in the northeastern margin of the Indochina block, SW China: Geochronological and petrogenetic constraints and implications for Gondwana assembly. *Precambrian Research* 245, 207-224.
- Qi, X.X., Zhu, L.H., Grimmer, J.C., Hu, Z.C., 2015. Tracing the Transhimalayan magmatic belt and the Lhasa block southward using zircon U–Pb, Lu–Hf isotopic and geochemical data: Cretaceous–Cenozoic granitoids in the Tengchong block, Yunnan, China. *Journal of Asian Earth Sciences* 110, 170-188.
- Qi, X.X., Santosh, M., Zhao, Y.H., Hu, Z.C., Zhang, C., Ji, F.B., Wei, C., 2016. Mid-Neoproterozoic ridge subduction and magmatic evolution in the northeastern margin of the Indochina block: Evidence from geochronology and geochemistry of calc-alkaline plutons. *Lithos* 248-251, 138-152.
- Qian, Q., Hermann, J., 2013. Partial melting of lower crust at 10–15 kbar: constraints on adakite and TTG formation. *Contributions to Mineralogy and Petrology* 165 (6), 1195–1224.
- Rampone, E., Hofmann, A.W., Piccardo, G.B., Vannucci, R., Bottazzi, P., Ottolini, L., 1995. Petrology, mineral and isotope geochemistry of the External Liguride peridotites (Northern Apennines, Italy). *Journal of Petrology* 36, 81–105.
- Rapp, R.P., Watson, E.B., 1995. Dehydration melting of Metabasalt at 8-32 kbar: Implications for continental growth and crust-mantle recycling. *Journal of Petrology* 36, 891-931.
- Roberts, M.P., Clemens, J.D., 1993. The origin of high-K, calc-alkaline, I-type granitoid magmas. *Geology* 21, 825-828.
- Rudnick, R.L., Gao, S., 2003. Composition of the continental crust. *Treatise on Geochemistry* 3,

1-64.

- Sarjoughian, F., Kananian, A., Haschke, M., Ahmadian, J., Ling, W., Keqing, Z., 2012. Magma mingling and hybridization in the Kuh-e Dom pluton, Central Iran. *Journal of Asian Earth Sciences* 54-55, 49-63.
- Searle, M.P., Noble, S.R., Cottle, J.M., Waters, D.J., Mitchell, A.H.G., Hlaing, T., Horstwood, M.S.A., 2007. Tectonic evolution of the Mogok metamorphic belt, Burma (Myanmar) constrained by U-Th-Pb dating of metamorphic and magmatic rocks. *Tectonics* 26, TC3014.
- Shellnutt, J.G., Jahn B.M., Zhou M.F., 2011. Crustally-derived granites in the Panzhihua region, SW China: Implications for felsic magmatism in the Emeishan large igneous province. *Lithos* 123, 145–157.
- Sheth, H.C., Torres-Alvarado, I.C., Verma, S.P., 2002. What Is the “Calc-alkaline Rock Series”? *International Geology Review* 44, 686-701.
- Shi, R.D., Griffin, W.L., O'Reilly, S.Y., Huang, Q.S., Zhang, X.R., Liu, D.L., Zhi, X.C., Xia, Q.X., Ding, L., 2012. Melt/mantle mixing produces podiform chromite deposits in ophiolites: Implications of Re–Os systematics in the Dongqiao Neo-tethyan ophiolite, northern Tibet. *Gondwana Research* 21, 194–206.
- Shi, Y.K., Jin, X.C., Huang, H., Yang, X.N., 2008. Permian fusulinids from the Tengchong block, western Yunnan, China. *The Paleontological Society* 82 (1), 118-127.
- Sisson, T.W., Ratajeski, K., Hankins, W.B., Glazner, A.F., 2005. Voluminous granitic magmas from common basaltic sources. *Contributions to Mineralogy and Petrology* 148, 635-661.
- Sreejith, C., Ravindra Kumar, G.R., 2013. Petrogenesis of high-K metagranites in the Kerala Khondalite Belt, southern India: a possible magmatic-arc link between India, Sri Lanka, and Madagascar. *Journal of Geodynamics* 63 (2013) 69-82.
- Stern, C.R. and Kilian, R., 1996. Role of the subducted slab, mantle wedge and continental crust in the generation of adakites from the Andean Austral Volcanic Zone. *Contribution to Mineralogy and Petrology* 123, 263-281.
- Stoltz, A.J., Jochum, K.P., Spettel, B., Hofmann, A.W., 1996. Fluid and melt-related enrichment in the subarc mantle: Evidence from Nd/Ta variations in island-arc basalts. *Geological Society of America* 24, 587-590.
- Stouraiti, C., Baziotis, I., Asimow, P.D., Downes, H., 2018. Geochemistry of the Serifos

- calc-alkaline granodiorite pluton, Greece constraining the crust and mantle contributions to I-type granitoids. *International Journal of Earth Sciences* 107, 1657–1688.
- Sun, S.S. and McDonough, W.F., 1989. Chemical and isotope systematics of oceanic basalts: Implications for mantle composition and processes. In: Saunders, A. D., eds. *Magmatism in Ocean Basins*. Geological Society [London] Special Publication 42, 313-345.
- Suzano, N., Becchio, R., Sola, A., Ortiz, A., Nieves, A., Quiroga, M., Fuentes, G., 2017. The role of magma mixing in the evolution of the Early Paleozoic calc-alkaline granitoid suites. Eastern magmatic belt, Puna, NW Argentina. *Journal of South American Earth Sciences* 76, 25-46.
- Sylvester, P.J., 1998. Post collisional strongly peraluminous granites. *Lithos* 45, 29-44.
- Tan, M. and Zhan, W.D., 1990. Preliminary research of ophiolite belt in south Nujiang belt, western Yunnan. *Exploration of Geosciences*. 3, 91-96 (in Chinese with English abstract).
- Tibet geological survey institute, 2001. Regional geological map and regional geology of Bange and Duoba region, scale 1:250000, Lhasa 15-281.
- Wang, C.M., Deng, J., Carranza, E.J.M., Santosh, M., 2014. Tin metallogenesis associated with granitoids in the southwestern Sanjiang Tethyan Domain: Nature, deposit types, and tectonic setting. *Gondwana Research* 26, 576-593.
- Wang, H.Z., Chen, P.R., Sun, L.Q., Ling, H.F., Zhao, Y.D., Lan, H.F., 2015. Magma mixing and crust–mantle interaction in Southeast China during the Early Cretaceous: Evidence from the Furongshan granite porphyry and mafic microgranular enclaves. *Journal of Asian Earth Sciences* 111, 72-87.
- Wang, Y., Zhang, X.M., Jiang, C.S., Wei, H.Q., Wan, J.L., 2007. Tectonic controls on the late Miocene–Holocene volcanic eruptions of the Tengchong volcanic field along the southeastern margin of the Tibetan plateau. *Journal of Asian Earth Sciences* 30, 375-389.
- Wang, Y.J., Xing, X.W., Cawood, P.A., Lai, S.C., Xia, X.P., Fan, W.M., Liu, H.C., Zhang, F.F., 2013. Petrogenesis of early Paleozoic peraluminous granite in the Sibumasu Block of SW Yunnan and diachronous accretionary orogenesis along the northern margin of Gondwana. *Lithos* 182-183, 67-85.
- Wang, Y.J., Li, S.B., Ma, L.Y., Fan, W.M., Cai, Y.F., Zhang, Y.H., Zhang, F.F., 2015. Geochronological and geochemical constraints on the petrogenesis of Early Eocene metagabbroic rocks in Nabang (SW Yunnan) and its implications on the Neotethyan slab

- subduction. *Gondwana Research* 27, 1474-1486.
- Weissman, A., Kessel, R., Navon, O., Stein, M. 2013. The petrogenesis of calc-alkaline granites from the Elat massif, Northern Arabian–Nubian shield. *Precambrian Research* 236, 252- 264.
- White, R.V., Tarney, J., Kerr, A.C., Saunders, A.D., Kempton, P.D., Pringle, M.S., Klaver, G.T., 1999. Modification of an oceanic plateau, Aruba, Dutch Caribbean: implications for the generation of continental crust. *Lithos* 46, 43-68.
- Wilson, M., 1989. Igneous petrogenesis: A global tectonic approach. Chapman & Hall, London, p 50-420.
- Woodhead, J., Hergt, J., Davidson, J., Eggins, S., 2001. Hafnium isotope evidence for “conservative” element mobility during subduction zone processes. *Earth and Planetary Science Letters* 192, 331-346.
- Wopfner, H., 1996. Gondwana origin of the Baoshan and Tengchong terranes of west Yunnan. Geological Society, London, Special Publications 106, 539-547.
- Wopfner, H., Jin, X.C., 2009. Pangea Megasequences of Tethyan Gondwana-margin reflect global changes of climate and tectonism in Late Palaeozoic and Early Triassic times-a review. *Palaeoworld* 18, 169-192.
- Xie, J.C., Zhu, D.C., Dong, G.C., Zhao, Z.D., Wang, Q., Mo, X.X., 2016. Linking the Tengchong Terrane in SW Yunnan with the Lhasa Terrane in southern Tibet through magmatic correlation. *Gondwana Research* 39, 217-229.
- Xu, Y.G., Yang, Q.J., Lan, J.B., Luo, Z.Y., Huang, X.L., Shi, Y.R., 2012. Temporal-spatial distribution and tectonic implications of the batholiths in the Gaoligong–Tengliang–Yingjiang area, western Yunnan: Constraints from zircon U–Pb ages and Hf isotopes. *Journal of Asian Earth Sciences* 53, 151-175.
- Xu, Z.Q., Wang, Q., Cai, Z.H., Dong, H.W., Li, H.Q., Chen, X.J., Duan, X.D., Cao, H., Li, J., Burg, J.P., 2015. Kinematics of the Tengchong Terrane in SE Tibet from the late Eocene to early Miocene: Insights from coeval mid-crustal detachments and strike-slip shear zones. *Tectonophysics* 665, 127-148.
- Yang, J.S., Xu, Z.Q., Duan, X.D., Li, J., Xiong, F.H., Liu, Z., Cai, Z.H., Li, H.Q., 2012. Discovery of a Jurassic SSZ ophiolite in the Myitkyina region of Myanmar. *Acta Petrologica Sinica*, 28(6): 1710-1730 (in Chinese with English abstract).

- Yang, Q.J., Xu, Y.G., Huang, X.L. and Luo, Z.Y., 2006. Geochronology and geochemistry of granites in the Gaoligong tectonic belt, western Yunnan: Tectonic implications. *Acta Petrologica Sinica* 22, 817-834 (in Chinese with English abstract).
- Yin, A. and Harrison, T.M., 2000. Geologic evolution of the Himalayan–Tibetan orogen. *Annual Review of Earth and Planetary Sciences* 28, 211-280.
- Yin, F.G., Zhang, H., Huang, Y., Ye, P.S., Yang, X.J., Lu, Y., Lin, S.L., 2012. Advances in the basic geological survey along Dali-Ruili section of Fanya railway, western Yunnan Province. *Geological Bulletin of China* 31(2/3), 218-226 (in Chinese with English abstract).
- Yunnan Bureau Geological Mineral Resource, 1991. *Regional Geology of Yunnan Province*. Geology Publication House, Beijing, pp. 1–729 (in Chinese with English abstract).
- Yunnan geological survey institute, 2011. Regional geological map and regional geology of Luxi region, scale 1:250000, Kunming 23-162.
- Zhang, K.J., Zhang, Y.X., Tang, X.C., Xia, B., 2012. Late Mesozoic tectonic evolution and growth of the Tibetan plateau prior to the Indo-Asian collision. *Earth Science Reviews* 114, 236-249.
- Zhang, K.J., Xia, B., Zhang, Y.X., Liu, W.L., Zeng, L., Li, J.F., Xu, L.F., 2014. Central Tibetan Meso-Tethyan oceanic plateau. *Lithos* 210-211, 278-288.
- Zhang, Q., 2014. Classifications of mafic-ultramafic rocks and their tectonic significance. *Chinese Journal of Geology* 49(3), 982-1017 (in Chinese with English abstract)
- Zhang, Y.C., Shi, G.R., Shen, S.Z., 2013. A review of Permian stratigraphy, paleobiogeography and palaeogeography of the Qinghai–Tibet Plateau. *Gondwana Research* 24, 55-76.
- Zhang, Y.C., Shen, S.Z., Zhang, Y.J., Zhu, T.X., An, X.Y., Huang, B.X., Ye, C.L., Qiao, F., Xu, H.P., 2018. Middle Permian foraminifers from the Zhabuye and Xiadong areas in the central Lhasa Block and their paleobiogeographic implications. *Journal of Asian Earth Sciences*, <https://doi.org/10.1016/j.jseaes.2018.01.008>.
- Zhang, Y.X., Li, Z.W., Yang, W.G., Zhu, L.D., Jin, X., Zhou, X.Y., Tao, G., Zhang, K.J. 2017. Late Jurassic–Early Cretaceous episodic development of the Bangong Meso-Tethyan subduction: Evidence from elemental and Sr–Nd isotopic geochemistry of arc magmatic rocks, Gaize region, central Tibet, China. *Journal of Asian Earth Sciences* 135, 212-242.
- Zhao, S.W., Lai, S.C., Qin, J.F., Zhu, R.Z., 2016. Tectono-magmatic evolution of the Gaoligong

- belt, southeastern margin of the Tibetan plateau: Constraints from granitic gneisses and granitoid intrusions. *Gondwana Research* 35, 238-256.
- Zhao, S.W., Lai, S.C., Qin, J.F., Zhu, R.Z., Wang, J.B., 2017. Geochemical and geochronological characteristics of Late Cretaceous to Early Paleocene granitoids in the Tengchong Block, Southwestern China: Implications for crustal anatexis and thickness variations along the eastern Neo-Tethys subduction zone. *Tectonophysics* 694, 87-100.
- Zhou, M.F., Robinson, P.T., Wang, C.Y., Jun-Hong Zhao, J.H., Yan, D.P., Gao, J.F., Malpas, J., 2012. Heterogeneous mantle source and magma differentiation of Quaternary arc-like volcanic rocks from Tengchong, SE margin of the Tibetan Plateau. *Contributions to Mineralogy and Petrology* 163, 841-860.
- Zhu, B.Q., Mao, C.X., Lugmair, G.W., Macdougall, J.D., 1983. Isotopic and geochemical evidence for the origin of Plio-Pleistocene volcanic rocks near the Indo-Eurasian collisional margin at Tengchong, China. *Earth and Planetary Science Letters* 65, 263-275.
- Zhu, D.C., Mo, X.X., Wang, L.Q., Zhao, Z.D., Niu, Y.L., Zhou, C.Y., Yang, Y.H., 2009. Petrogenesis of highly fractionated I-type granites in the Zayu area of eastern Gangdese, Tibet: Constraints from zircon U-Pb geochronology, geochemistry and Sr-Nd-Hf isotopes. *Science. China Earth Sciences.* 52 (9), 1223-1239.
- Zhu, D.C., Mo, X.X., Zhao, Z.D., Niu, Y.L., Wang, L.Q., Chu, Q.H., Pan G.T., Xu, J.F., Zhou, C.Y., 2010. Presence of Permian extension- and arc-type magmatism in southern Tibet: Paleogeographic implications. *Geological Society of America Bulletin* 122, 979-993.
- Zhu, D.C., Zhao, Z.D., Niu, Y.L., Mo, X.X., Chung, S.L., Hou, Z.Q., Wang, L.Q., Wu, F.Y., 2011. The Lhasa Terrane: Record of a microcontinent and its histories of drift and growth. *Earth and Planetary Science Letters* 301, 241-255.
- Zhu, D.C., Zhao, Z.D., Niu, Y.L., Dilek, Y., Hou, Z.Q., Mo, X.X., 2013. The origin and pre-Cenozoic evolution of the Tibetan Plateau. *Gondwana Research* 23, 1429-1454.
- Zhu, D.C., Li, S.M., Cawood, P.A., Wang, Q., Zhao, Z.D., Liu, S.A., Wang, L.Q., 2016. Assembly of the Lhasa and Qiangtang terranes in central Tibet by divergent double subduction. *Lithos* 245, 7-17.
- Zhu, R.Z., Lai, S.C., Qin, J.F., Zhao, S.W., 2015. Early-Cretaceous highly fractionated I-type granites from the northern Tengchong block, western Yunnan, SW China: Petrogenesis and

tectonic implications . Journal of Asian Earth Sciences 100, 145-163.

- Zhu, R.Z., Lai, S.C., Santosh, M., Qin, J.F., Zhao, S.W., 2017. Early Cretaceous Na-rich granitoids and their enclaves in the Tengchong Block, SW China: Magmatism in relation to subduction of the Bangong–Nujiang Tethys ocean. *Lithos* 286–287, 175–190.
- Zou, G.F., Mao, Y., Lin, S.L., Cong, F., Li, Z.H., Xie, T., Gao, Y.J., 2013. Zircon U-Pb age and geochemistry of Mengyang instrusion and its tectonic implicans in the Lianghe, western Yunnan. *Journal of Mineral Petrology* 3, 87-99 (in Chinese with English abstract).

### Figure captions

Fig. 1. Simplified geological map of the Transhimalayan magmatic belt in the Himalaya–Tibet tectonic realm (modified from Ji et al., 2009, Wang et al., 2013, and Xu et al., 2015). Inset shows the location of Fig. 2 in the Himalaya–Tibet tectonic realm. MBT = Main Boundary Thrust; YTS = Yarlung–Tsangpo Suture; BNS = Bangong–Nujiang Suture; IBS = Indo–Burma Suture; MK = Myitkyina Suture; KY = Kalaymyo Suture; SL, CL, NL = South, Central, North Lhasa blocks; GLG = Gaoligong Orogen.

Fig. 2. Geological map of the Gaoligong Orogen showing the major geologic units, sample localities, new U–Pb zircon age data of this study (black circles), and other age data (white circles, from Yang et al., 2006, Cong et al., 2011, Qi et al., 2011, Xu et al., 2012, Yin et al., 2012, and Xie et al., 2016). The map was modified after Qi et al. (2015). DYJF = Dayingjiang Fault; LCJF = Longchuanjiang Fault; LLRF = Lushui–Longling–Ruili Fault.

Fig. 3. Representative field photographs and photomicrographs of rocks from the plutons in the Gaoligong Orogen. (a) and (b) Anhedral laths of hornblende (Hb) in

the gabbroic diorite, some of which have residual pyroxene (Py) cores. (c) Example of an MME hosted within the granodiorite, with a transitional and leucocratic zone at the contact. (d) Right side shows an MME with typical igneous textures and without cumulate textures. Left side shows the coarse-grained granodiorite. (e) and (f) Subhedral to anhedral laths of plagioclase (Pl) that occur as inclusions in K-feldspar (Kf). The plagioclase laths have compositional zoning and resorbed borders.

Fig. 4. (a) TAS classification and (b)  $K_2O$  vs.  $SiO_2$  diagrams (e.g., Le Maitre et al., 1989). The shaded bands are the fields with boundary lines of Peccerillo and Taylor (1976). (c)  $Na_2O + K_2O - CaO$  vs.  $SiO_2$  and (d)  $FeO/(FeO + MgO)$  vs.  $SiO_2$  diagrams (e.g., Frost et al., 2001).

Fig. 5. Chondrite-normalized REE patterns and primitive-mantle-normalized trace element spider diagrams for the plutonic rocks of the Gaoligong Orogen. Chondrite and primitive mantle values are from Sun and McDonough (1989).

Fig. 6. CL images and U–Pb ages of analytical spots in zircons from the plutonic rocks of the Gaoligong Orogen. The scale bar is 100  $\mu m$ . (a) and (b) are from diorites; (c)–(e) are from granodiorites; (f)–(j) are from granites.

Fig. 7. U–Pb concordia diagrams for zircons from the plutonic rocks in the Gaoligong Orogen. The red lines in (f), (i), and (j) are not calculated, and (h) is calculated alone.

Fig. 8. Histograms of  $\epsilon_{Hf}(t)$  values and  $T_{DM}^C$  ages for zircons from plutonic rocks of

the Gaoligong Orogen.

Fig. 9. (a) Plots of  $\varepsilon_{\text{Hf}}(t)$  versus U–Pb ages for zircons from plutonic rocks in the Gaoligong Orogen. (b) Histogram of  $T_{\text{DM}}^{\text{C}}$  ages. Reference line representing chondritic Hf evolution (CHUR) is from Blichert-Toft and Albarede (1997). Data for the Bangonghu–Nujiang Suture (BNS) are from Zhu et al. (2016).

Fig. 10.  $\text{Mg}^{\#}$  vs  $\text{SiO}_2$  diagram the plutonic rocks in the Gaoligong Orogen. Fields shown are as follows: pure crustal partial melts obtained in experimental studies by dehydration melting of low-K basaltic rocks at 8–16 kbar and 1000–1050 °C (e.g., Rapp and Watson, 1995); pure crustal melts obtained in experimental studies by the moderately hydrous (1.7–2.3 wt.%  $\text{H}_2\text{O}$ ) melting of medium- to high-K basaltic rocks at 7 kbar and 825–950 °C (e.g., Sisson et al., 2005); mantle melts (basalts); and Quaternary volcanic rocks from the Andean southern volcanic zone (e.g., Lopez-Escobar et al., 1993). The curve for mantle AFC was calculated following Depaolo (1981) with a mass assimilation/fractionation ratio of  $r = 2$ , reflecting a relatively hot mantle wedge, and 80% amphibole + 20% clinopyroxene as the fractionating phases (e.g., Stern and Kilian, 1996).

Fig. 11. Th/Yb vs. Ba/La and Th/Yb vs. Sr/Nd discrimination diagrams for the plutonic rocks in the Gaoligong Orogen.

Fig. 12. Variation diagrams for the plutonic rocks in the Gaoligong Orogen.

Fig. 13 Initial magma evolutionary paths of the granitoids by rhyolite-MELTS (a-c)

and Binary mixing model based on Na<sub>2</sub>O/CaO vs. MgO/Al<sub>2</sub>O<sub>3</sub> (d). (a), (b) and (c) The initial magma evolutionary paths of the granitoids by rhyolite-MELTS based on the average geochemical compositions of the lower-, middle-, and upper crust from Rudnick and Gao (2003). (d) The mixing line was calculated assuming a pure crustal melt from S type granitic sample (15QML-5) and a pure mantle-derived melt represented by early Cretaceous basalt from Bangong-Nujiang suture.

Fig. 14. Discrimination diagrams for the tectonic settings of the plutons. (a) and (b) from Pearce et al. (1984), (c) from Pearce et al. (1977), and (d) from Harris et al. (1986). VAG = volcanic arc granites, S-COLG = syn-collisional granites, P-COLG = post-collisional granites, WPG = within-plate granites, ORG = oceanic ridge granites, and A-ORG = abnormal oceanic ridge granites.

Fig. 15. Schematic model of the evolution of magmas in relation to subduction of oceanic lithosphere. The fluids released from the subducted slab and overlying sediments as a result of multistage dehydration migrated upwards through the overlying mantle wedge, resulting in metasomatism and melting of the mantle wedge. The mantle-derived magma was injected into the overlying crust, resulting in the partial melting of crustal rocks to produce granitic magma. The mafic magmas mixed with the crustal melts in different proportions to produce various dioritic and granitoid magmas. The mélange was formed due to the tectonic mixing of materials from the oceanic and continental crusts.

### Table captions

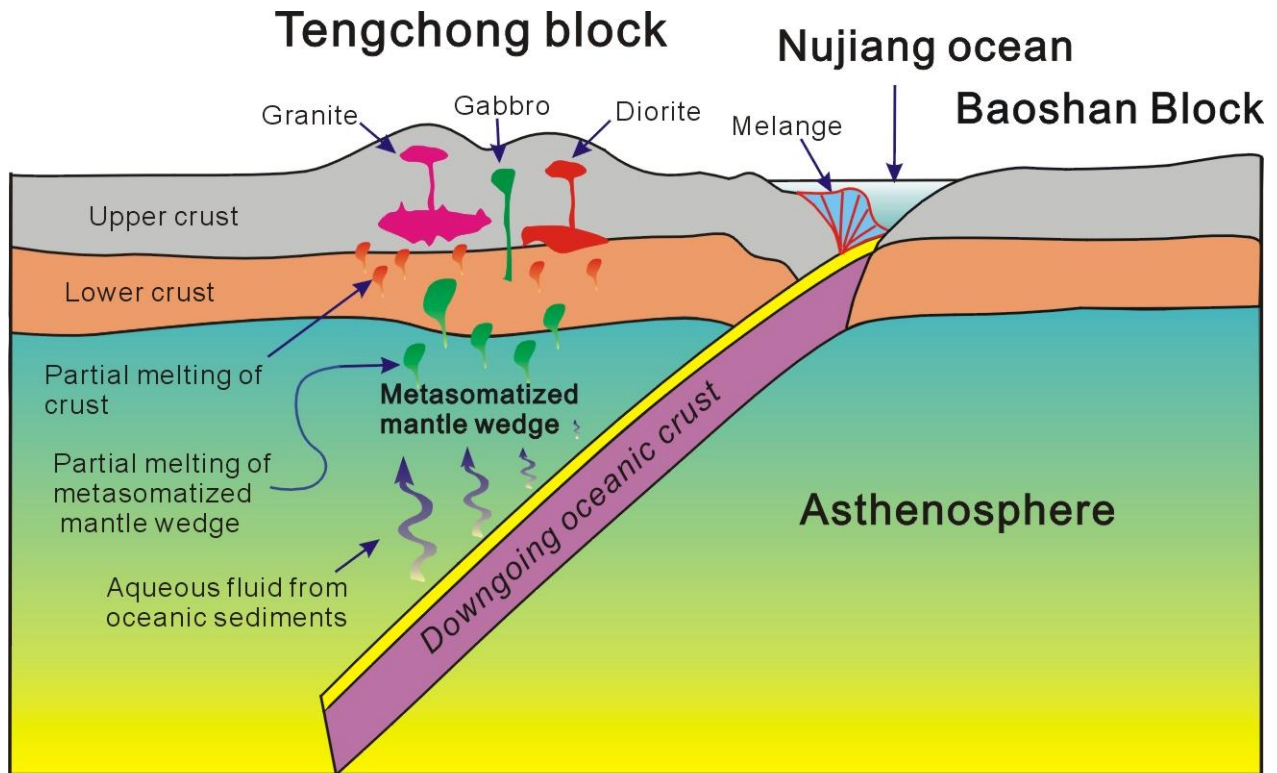
Table 1. Major and trace element compositions of the plutonic rocks in the Gaoligong Orogen.

Note: Mg<sup>#</sup> = 100 × molecular Mg<sup>2+</sup>/(Mg<sup>2+</sup> + Fe<sup>2+</sup> + Fe<sup>3+</sup>); A/NK=molecular Al<sub>2</sub>O<sub>3</sub> / (Na<sub>2</sub>O+K<sub>2</sub>O), A/CNK=molecular Al<sub>2</sub>O<sub>3</sub> / (CaO+Na<sub>2</sub>O+K<sub>2</sub>O), show the Al saturation; REE = rare earth element; Eu/Eu\* = Eu<sub>N</sub>/(Sm<sub>N</sub> + Gd<sub>N</sub>)<sup>1/2</sup>, shows the change of the anomaly, with the subscript N denoting a normalization to chondrite (e.g., Sun and McDonough, 1989); (La/Sm)<sub>N</sub> represents the degree of light REE fractionation.

Table 2. Zircon LA–ICP–MS U–Pb data for plutonic rocks of the Gaoligong Orogen.

Table 3. Zircon LA–ICP–MS Lu–Hf isotope data for plutonic rocks of the Gaoligong Orogen.

Graphical abstract



Graphical abstract

ACCEPTED

**Highlights**

- Early Cretaceous diorites are identified for the first time in the Gaoligong Orogen.
- The rocks were produced by mixing of the mantle- and crust-derived melts in an arc setting.
- The Gaoligong orogen is the southward extension of the Bangonghu-Nujiang suture.

Table 1

Rocks	Monzodiorite ( $\delta_1$ ) (25°58'59"N, 98°42'26"E)				gabbroic diorite ( $\delta_2$ ) (24°31' 37" N, 98°12' 11" E)				
Sample	15QLP-39	15QLP-40	15QLP-42	15QLP-43	15QML-65	15QML-66	15QML-67	15QML-68	15QML-69
<b>Major element (%)</b>									
SiO <sub>2</sub>	51.53	51.56	50.95	51.92	52.19	53.25	54.16	53.31	54.11
TiO <sub>2</sub>	2.30	2.26	2.30	2.24	1.44	0.80	0.85	0.96	0.79
Al <sub>2</sub> O <sub>3</sub>	15.99	15.79	15.85	15.80	15.21	16.71	15.44	15.67	16.31
Fe <sub>2</sub> O <sub>3</sub>	2.19	2.00	2.03	2.66	3.37	2.05	2.22	2.90	2.72
FeO	7.35	7.60	7.73	6.96	6.30	4.63	5.18	5.26	4.27
MnO	0.16	0.16	0.16	0.16	0.17	0.13	0.14	0.16	0.14
MgO	5.29	5.36	5.53	5.24	6.08	6.84	7.25	6.52	7.03
CaO	7.17	7.05	7.22	7.01	9.12	9.60	9.33	9.61	9.56
Na <sub>2</sub> O	3.26	3.17	3.16	3.20	2.72	2.72	2.68	2.77	2.72
K <sub>2</sub> O	2.20	2.34	2.32	2.29	0.84	0.87	0.61	0.66	0.54
P <sub>2</sub> O <sub>5</sub>	0.23	0.24	0.22	0.25	0.06	0.08	0.09	0.08	0.10
CO <sub>2</sub>	0.10	0.10	0.15	0.10	0.15	0.10	0.20	0.30	0.4
H <sub>2</sub> O <sup>+</sup>	1.46	2.02	1.46	1.48	1.42	1.52	1.62	1.42	1.60
LOI	0.66	0.61	0.65	0.58	0.95	1.21	1.22	1.02	1.21
A/NK	2.06	2.04	2.06	2.04	2.82	3.08	3.05	2.97	3.22
A/CNK	0.77	0.77	0.76	0.77	0.69	0.73	0.70	0.69	0.73
Mg <sup>#</sup>	53.1	52.9	53.3	53.4	58.1	68.7	67.7	63.9	69.5
<b>REE(ppm)</b>									
La	25.4	22.4	22.1	25.9	10.4	9.83	10.0	10.3	9.76
Ce	65.2	57.5	57.6	63.9	23.7	24.0	22.4	24.8	22.6
Pr	8.49	7.74	6.93	7.87	3.01	2.66	2.79	3.00	2.73
Nd	35.0	33.2	30.4	33.3	14.6	11.7	13.3	12.9	12.8
Sm	8.12	7.43	6.80	7.43	3.44	3.04	3.01	3.35	2.97
Eu	2.26	2.03	1.90	1.97	1.15	0.98	1.00	1.07	0.91
Gd	8.91	7.69	7.69	7.66	4.07	3.63	3.52	4.22	3.33
Tb	1.43	1.35	1.22	1.29	0.72	0.60	0.61	0.66	0.60
Dy	8.21	7.37	7.06	7.17	4.45	3.83	3.80	4.12	3.72
Ho	1.57	1.48	1.29	1.35	0.92	0.72	0.78	0.79	0.77
Er	4.34	3.80	3.68	3.67	2.61	2.12	2.09	2.29	2.10
Tm	0.60	0.57	0.52	0.54	0.36	0.31	0.31	0.36	0.28
Yb	3.86	3.55	3.18	3.46	2.41	2.01	2.10	2.11	1.89
Lu	0.59	0.50	0.49	0.48	0.35	0.30	0.29	0.31	0.30
$\Sigma$ REE	174	157	151	166	72	66	66	70	65
LREE/HREE	4.90	4.95	5.00	5.48	3.54	3.86	3.89	3.73	3.99
Eu/Eu*	0.81	0.81	0.80	0.79	0.94	0.90	0.94	0.87	0.88
(La/Sm) <sub>N</sub>	2.02	1.95	2.10	2.25	1.95	2.09	2.14	1.98	2.12

## Trace element (ppm)

Rb	110	138	161	96.1	40.9	41.9	29.0	29.1	24.4
Ba	292	263	261	274	233	172	221	179	144
Th	5.63	5.22	4.64	5.91	2.66	2.87	2.63	2.85	3.08
U	0.77	0.74	0.66	0.75	0.48	0.41	0.39	0.47	0.41
Nb	20.3	18.1	18.6	20.0	3.63	2.74	3.05	2.88	2.85
Ta	1.30	1.18	1.09	1.20	0.25	0.20	0.20	0.24	0.20
Sr	405	321	351	331	214	220	210	216	241
Zr	194	203	188	208	108	86.1	85.5	80.9	84.6
Hf	6.17	6.2	5.42	6.05	3.13	2.55	2.53	2.49	2.34
Y	36.8	33.7	34.8	34.4	22.5	17.5	19.3	20.4	20.2
Ni	69.1	61.2	65.9	60.6	34.2	67.3	47.3	27.3	54.2
Sc	24.7	21.3	21.3	21.4	36.2	29.4	30.9	35.4	32.3

Continuous Table 1

Rocks	granodiorite ( $\gamma\delta_1$ ) (24°38'1"N, 98°31'15"E)					granodiorite ( $\gamma\delta_2$ ) (24°14'41"N, 98°0'33"E)				
Sample	15QMH-1	15QMH-2	15QMH-3	15QMH-4	15QMH-5	15QLL-21	15QLL-22	15QLL-23	15QLL-24	15QLL-25
Major element (%)										
SiO <sub>2</sub>	65.50	64.30	64.23	63.54	63.90	65.39	66.32	66.01	64.15	66.33
TiO <sub>2</sub>	0.55	0.63	0.58	0.58	0.59	0.64	0.60	0.62	0.70	0.62
Al <sub>2</sub> O <sub>3</sub>	15.45	15.79	15.80	16.20	15.20	15.94	15.64	15.89	16.20	15.66
Fe <sub>2</sub> O <sub>3</sub>	4.53	4.73	4.21	4.23	4.40	2.43	2.49	1.42	1.27	2.03
FeO	3.38	3.21	2.64	2.73	2.75	2.08	1.64	1.94	2.58	2.27
MnO	0.07	0.09	0.07	0.08	0.08	0.07	0.07	0.06	0.07	0.07
MgO	1.89	2.30	2.07	2.08	2.04	1.34	1.25	1.37	1.59	1.35
CaO	3.22	4.49	3.70	4.58	4.47	3.67	3.81	3.44	3.42	3.87
Na <sub>2</sub> O	3.74	3.57	3.38	3.59	3.19	3.57	3.51	3.26	3.03	3.52
K <sub>2</sub> O	1.87	1.65	3.00	2.46	2.80	2.77	2.58	3.98	4.85	2.46
P <sub>2</sub> O <sub>5</sub>	0.14	0.16	0.15	0.15	0.15	0.15	0.15	0.23	0.25	0.15
CO <sub>2</sub>	0.55	0.32	0.45	0.70	0.86	0.10	0.10	0.10	0.10	0.10
H <sub>2</sub> O <sup>+</sup>	2.36	1.64	2.34	1.94	2.12	0.94	1.04	0.86	0.96	0.86
LOI	0.77	1.16	1.27	1.19	1.34	0.76	0.80	0.73	0.77	0.66
A/NK	1.89	2.06	1.79	1.89	1.84	1.80	1.83	1.64	1.58	1.85
A/CNK	1.10	1.00	1.02	0.96	0.93	1.03	1.01	1.00	0.98	1.01
Mg <sup>#</sup>	38.3	43.4	44.9	44.5	43.5	42.9	44.7	48.6	47.4	43.1
REE(ppm)										
La	36.3	43.7	28.1	21.3	46.8	30.2	39.5	87.4	94.7	36.5
Ce	54.3	73.9	46.8	41.7	72.2	65.5	80.7	163.0	196.0	77.3
Pr	6.08	9.23	6.00	5.87	7.98	7.20	8.33	16.10	18.70	8.48
Nd	22.9	38.70	27.2	25.9	31.0	26.8	31.8	55.7	69.2	34.6
Sm	3.17	7.04	4.56	5.11	5.01	5.10	5.95	8.04	11.80	6.44
Eu	0.83	1.23	1.08	1.14	1.14	1.20	1.30	1.28	1.76	1.26

Gd	2.59	6.20	3.94	4.61	4.22	4.77	5.26	5.78	9.50	5.91
Tb	0.31	0.84	0.55	0.66	0.59	0.86	0.93	1.05	1.63	1.03
Dy	1.62	4.72	3.29	3.82	3.18	4.60	5.14	5.09	8.41	5.79
Ho	0.34	0.91	0.69	0.77	0.66	0.88	0.99	0.92	1.53	1.10
Er	0.94	2.46	1.91	2.29	1.89	2.43	2.75	2.70	4.22	3.31
Tm	0.14	0.32	0.28	0.32	0.27	0.37	0.44	0.37	0.56	0.46
Yb	0.90	2.09	1.83	2.13	1.82	2.24	2.68	2.33	3.59	2.84
Lu	0.14	0.29	0.28	0.32	0.28	0.32	0.38	0.32	0.50	0.39
$\Sigma$ REE	131	192	127	116	177	152	186	350	422	185
LREE/ HREE	17.70	9.75	8.91	6.77	12.71	8.26	9.02	17.86	13.10	7.90
Eu/Eu*	0.86	0.56	0.76	0.70	0.74	0.73	0.70	0.55	0.49	0.61
(La/Sm) <sub>N</sub>	7.39	4.01	3.98	2.69	6.03	3.82	4.29	7.02	5.18	3.66
Trace element (ppm)										
Rb	78.7	62.0	143	90.9	158	130	133	184	186	119
Ba	278	475	646	555	601	564	554	900	1164	497
Th	16.7	12.2	10.5	14.4	19.2	12.8	14.0	37.6	41.0	19.2
U	1.93	1.5	2.04	2.29	2.76	1.69	1.57	2.24	2.48	2.26
Nb	7.75	11	9.33	9.45	9.2	18.5	14.5	17.7	23.9	20.7
Ta	0.52	0.88	0.78	0.84	0.81	1.06	1.09	1.09	1.7	1.21
Sr	309	374	374	429	423	256	265	371	355	288
Zr	147	128	122	132	113	217	192	248	361	211
Hf	4.25	4.56	4.18	4.33	3.83	6.26	6.05	7.75	11.1	6.24
Y	9.90	23.0	18.4	21.4	18.2	23.0	23.5	23.6	36.6	29.3
Ni	11.9	13.2	10.7	12.7	11.8	4.1	4.92	10.4	8.83	4.74
Sc	6.40	16.0	9.80	11.3	10.2	9.03	9.61	6.85	10.1	9.81

Continuous Table 1

Rocks	granodiorite ( $\gamma_3$ ) (24°31'6"N, 98°17'10"E)					granite ( $\gamma_1$ ) (24°52'56"N, 98°42'43"E)			
	Sample	15QML-57	15QML-58	15QML-59	15QML-60	15QML-61	10QTG-38	10QTG-39	10QTG-40
Major element (%)									
SiO <sub>2</sub>	66.08	66.65	70.85	70.28	68.77	70.31	71.88	69.62	70.33
TiO <sub>2</sub>	0.60	0.53	0.36	0.37	0.44	0.36	0.32	0.30	0.32
Al <sub>2</sub> O <sub>3</sub>	17.00	16.14	15.20	15.71	15.99	14.58	14.25	15.77	14.84
Fe <sub>2</sub> O <sub>3</sub>	1.25	1.65	0.69	0.78	1.51	0.39	0.35	0.41	0.44
FeO	2.18	2.34	1.46	1.39	1.72	2.10	1.83	1.69	1.83
MnO	0.07	0.08	0.06	0.05	0.07	0.08	0.06	0.06	0.07
MgO	1.59	1.65	1.00	1.07	1.12	0.80	0.70	0.62	0.72
CaO	4.19	3.80	3.11	3.38	3.71	2.16	2.30	2.08	2.19
Na <sub>2</sub> O	4.37	3.99	3.86	4.11	4.34	3.16	3.36	3.26	3.26
K <sub>2</sub> O	1.68	1.88	2.39	2.09	1.58	4.91	3.94	4.98	4.85
P <sub>2</sub> O <sub>5</sub>	0.24	0.16	0.08	0.13	0.13	0.08	0.07	0.06	0.07

CO <sub>2</sub>	0.10	0.10	0.10	0.10	0.10	0.44	0.36	0.40	0.44
H <sub>2</sub> O <sup>+</sup>	0.86	0.82	0.78	0.74	0.76	0.17	0.26	0.17	0.17
LOI	0.44	0.51	0.58	0.56	0.51	0.33	0.42	0.50	0.45
A/NK	1.89	1.88	1.70	1.74	1.81	1.39	1.45	1.47	1.40
A/CNK	1.02	1.04	1.04	1.04	1.03	1.01	1.02	1.08	1.02
Mg <sup>#</sup>	50.8	48.8	50.2	52.3	45.4	38.5	38.6	37.1	38.8
REE(ppm)									
La	11.7	29.2	21.2	17.1	39.2	36.0	48.4	42.7	42.8
Ce	24.5	60.1	44.0	32.9	79.1	66.6	86.2	77.5	79.3
Pr	2.68	5.96	4.35	3.46	7.54	7.43	9.81	9.95	9.19
Nd	12.2	21.8	16.7	13.6	28.1	26.5	34.1	35.4	32.0
Sm	2.52	4.21	3.46	3.00	5.16	4.78	6.27	6.51	6.33
Eu	0.98	1.09	0.92	1.02	0.83	0.84	0.90	0.84	0.91
Gd	2.53	4.07	3.15	2.93	4.69	4.56	5.50	5.37	5.72
Tb	0.48	0.60	0.50	0.49	0.76	0.80	0.98	0.88	1.04
Dy	2.54	3.27	2.95	2.42	4.23	4.91	5.89	5.02	6.58
Ho	0.51	0.55	0.53	0.46	0.77	0.99	1.22	0.98	1.31
Er	1.33	1.45	1.47	1.12	2.00	3.08	3.85	3.19	4.20
Tm	0.16	0.18	0.19	0.12	0.27	0.45	0.54	0.45	0.57
Yb	0.88	1.01	1.12	0.73	1.67	3.02	3.66	2.88	3.83
Lu	0.14	0.16	0.16	0.10	0.24	0.44	0.50	0.43	0.56
ΣREE	63	134	101	79	175	160	208	192	194
LREE/ HREE	6.37	10.84	9.00	8.49	10.93	7.79	8.39	9.01	7.16
Eu/Eu*	1.17	0.79	0.84	1.04	0.51	0.54	0.46	0.42	0.45
(La/Sm) <sub>N</sub>	3.00	4.48	3.96	3.68	4.90	4.86	4.98	4.23	4.36
Trace element (ppm)									
Rb	80.0	100	93.0	81.9	72.1	223	198	240	238
Ba	327	337	553	530	311	453	373	590	501
Th	2.04	7.50	7.89	4.10	15.0	21.2	38.5	27.4	33.2
U	1.03	0.73	1.01	1.34	2.01	2.85	5.16	2.91	3.42
Nb	2.64	5.57	6.00	4.20	7.13	12.7	13.2	11.6	14.3
Ta	0.42	0.58	0.54	0.35	0.73	1.40	1.67	1.20	1.62
Sr	285	428	440	487	441	159	167	188	191
Zr	155	190	119	114	158	115	94.5	151	118
Hf	4.29	5.48	4.12	3.67	4.77	3.25	2.87	3.97	3.32
Y	12.6	14.3	13.1	11.0	18.2	29.9	33.9	29.0	39.3
Ni	8.58	8.73	8.59	10.7	4.53	2.91	3.08	2.99	3.27
Sc	12.2	11.7	4.54	8.20	3.15	7.31	5.77	5.09	6.47

Continuous Table 1

Rocks	granite ( $\gamma_2$ ) (24°26'33"N, 98°23'14"E)	granite ( $\gamma_3$ ) (24°27'45"N, 98°16'8"E)
-------	---	--

Sample	15QML-5	15QML-6	15QML-7	15QML-8	15QML-9	15QML-83	15QML-84	15QML-85	15QML-86	15QML-87
<b>Major element (%)</b>										
SiO <sub>2</sub>	74.48	76.19	76.28	72.18	76.49	73.16	74.29	74.41	74.05	74.87
TiO <sub>2</sub>	0.18	0.11	0.12	0.24	0.12	0.22	0.21	0.22	0.17	0.20
Al <sub>2</sub> O <sub>3</sub>	13.18	12.64	12.87	14.33	12.80	13.96	13.23	13.14	13.69	13.15
Fe <sub>2</sub> O <sub>3</sub>	0.44	0.12	0.19	0.34	0.16	1.00	1.08	1.19	0.98	1.13
FeO	1.65	0.90	0.82	2.29	0.70	0.73	0.51	0.50	0.43	0.44
MnO	0.06	0.03	0.02	0.11	0.02	0.04	0.03	0.04	0.03	0.04
MgO	0.50	0.23	0.24	0.53	0.20	0.37	0.33	0.35	0.28	0.32
CaO	0.89	0.84	0.85	1.45	0.87	1.69	1.51	1.56	1.64	1.48
Na <sub>2</sub> O	2.41	2.29	2.37	2.66	2.39	3.16	2.96	2.95	3.14	2.95
K <sub>2</sub> O	4.61	5.66	5.61	4.51	5.60	4.28	4.42	4.18	4.25	4.45
P <sub>2</sub> O <sub>5</sub>	0.03	0.03	0.03	0.04	0.03	0.05	0.05	0.05	0.04	0.05
CO <sub>2</sub>	0.10	0.10	0.14	0.10	0.10	0.15	0.10	0.10	0.10	0.10
H <sub>2</sub> O <sup>+</sup>	1.26	0.66	0.76	0.94	1.06	0.78	0.70	0.78	0.62	0.62
LOI	1.22	0.75	0.72	1.06	0.54	0.78	0.72	0.72	0.78	0.67
A/NK	1.47	1.28	1.29	1.55	1.28	1.42	1.37	1.40	1.40	1.36
A/CNK	1.25	1.11	1.12	1.20	1.11	1.08	1.07	1.08	1.07	1.06
Mg <sup>#</sup>	32.5	30.1	32.1	27.9	31.6	35.9	37.1	37.6	36.4	37.6
<b>REE(ppm)</b>										
La	55.5	40.7	41.0	79.1	40.1	32.9	32.9	30.7	41.3	24.2
Ce	126	94.9	88.5	168	90.6	68.2	68.8	63.6	88.5	49.8
Pr	12.6	9.81	9.52	17.8	9.90	7.52	7.26	6.45	8.59	5.24
Nd	44.8	37.1	38.6	65.8	37.0	25.6	25.3	23.1	31.8	19.7
Sm	8.91	7.04	6.50	11.8	6.96	4.96	5.10	4.35	5.68	3.87
Eu	0.77	0.65	0.73	0.99	0.76	0.58	0.57	0.63	0.63	0.57
Gd	8.02	5.68	5.36	10.3	5.77	4.93	4.95	3.82	4.26	3.55
Tb	1.27	0.93	0.92	1.84	0.91	0.73	0.79	0.64	0.77	0.56
Dy	7.73	5.08	4.70	9.33	4.45	4.04	4.09	3.58	3.89	3.29
Ho	1.43	1.03	0.93	1.94	0.81	0.69	0.69	0.62	0.72	0.59
Er	4.35	3.28	2.97	5.47	2.29	1.96	1.85	1.74	1.96	1.73
Tm	0.71	0.51	0.45	0.85	0.33	0.27	0.25	0.25	0.28	0.25
Yb	4.75	3.40	2.97	6.35	2.23	1.63	1.57	1.50	1.86	1.59
Lu	0.75	0.58	0.46	0.88	0.33	0.25	0.23	0.23	0.27	0.25
ΣREE	278	211	204	380	202	154	154	141	191	115
LREE/HREE	8.57	9.28	9.85	9.29	10.82	9.64	9.70	10.41	12.60	8.75
E/Eu*	0.27	0.30	0.37	0.27	0.36	0.35	0.34	0.46	0.16	0.46
(La/Sm) <sub>N</sub>	4.02	3.73	4.07	4.33	3.72	4.28	4.16	4.56	3.60	4.04
<b>Trace element (ppm)</b>										
Rb	137	171	163	163	179	202	204	182	182	195
Ba	538	326	393	531	350	449	435	407	400	384
Th	43.8	36.8	35.4	54.1	34.5	31.6	28.3	31.7	43.7	27.5
U	2.97	3.16	3.21	3.53	3.01	1.8	1.61	1.7	2.25	1.72

Nb	10.5	5.68	5.75	12.7	5.42	12.9	12.3	8.36	6.91	8.02
Ta	0.53	0.39	0.41	0.65	0.38	0.71	0.78	0.68	0.74	0.71
Sr	69.7	60.2	57.8	70.2	57.2	98.4	90.7	97.8	94.5	91.6
Zr	158	119	117	295	146	123	117	123	99	126
Hf	6.03	4.94	4.94	10.8	5.82	4.14	3.82	4.2	3.85	4.39
Y	36.7	25.9	23.5	43.2	20.4	19.2	18.9	17.7	17.8	17.4
Ni	1.54	0.6	0.87	1.88	1.89	1.42	1.21	1.96	1.51	2.03
Sc	6.18	3.07	3	9.12	2.31	4.49	4.47	4.35	3.22	4.10

Continuous Table 1

Rocks	granite ( $\gamma_4$ ) (24°3'57"N, 97°50'14"E)					granite ( $\gamma_5$ ) (22°57'39"N, 103°11'8"E)			
Sample	15QLR-5	15QLR-6	15QLR-7	15QLR-8	16QLM-1	16QLM-2	16QLM-3	16QLM-4	16QLM-5
Major element (%)									
SiO <sub>2</sub>	70.97	70.93	69.82	70.68	75.63	74.85	74.11	74.09	72.51
TiO <sub>2</sub>	0.40	0.36	0.43	0.39	0.20	0.19	0.21	0.25	0.28
Al <sub>2</sub> O <sub>3</sub>	14.36	14.25	14.48	14.19	12.46	13.79	13.49	13.41	13.88
Fe <sub>2</sub> O <sub>3</sub>	0.55	0.67	1.02	0.82	0.42	0.46	0.84	0.66	1.15
FeO	2.26	1.94	2.08	2.07	0.88	0.88	0.56	0.99	0.74
MnO	0.07	0.08	0.09	0.08	0.04	0.04	0.03	0.05	0.04
MgO	1.36	1.22	1.50	1.36	0.39	0.41	0.40	0.49	0.53
CaO	3.00	2.85	3.24	3.00	1.30	1.47	1.50	1.55	1.55
Na <sub>2</sub> O	3.25	3.18	3.32	3.12	2.68	3.20	3.00	2.96	3.05
K <sub>2</sub> O	3.32	3.74	3.27	3.59	4.61	4.56	4.79	4.61	4.92
P <sub>2</sub> O <sub>5</sub>	0.10	0.09	0.10	0.10	0.04	0.05	0.05	0.05	0.06
CO <sub>2</sub>	0.10	0.12	0.10	0.10	0.17	0.17	0.17	0.17	0.17
H <sub>2</sub> O <sup>+</sup>	0.62	0.66	0.64	0.60	0.69	0.41	0.57	0.28	0.86
LOI	0.33	0.43	0.33	0.43	0.52	0.53	0.67	0.33	0.76
A/NK	1.61	1.54	1.61	1.57	1.33	1.35	1.33	1.36	1.34
A/CNK	1.00	0.99	0.97	0.98	1.06	1.07	1.05	1.06	1.05
Mg <sup>#</sup>	49.2	49.2	51.3	49.9	39.4	40.2	43.2	40.4	42.9
REE(ppm)									
La	43.9	31.3	48.2	55.1	42.6	25.2	25.7	38.7	28.9
Ce	85.0	64.2	97.0	107.0	80.5	47.5	51.3	75.3	57.9
Pr	8.20	6.26	8.88	10.5	8.39	5.07	5.82	8.18	6.62
Nd	29.6	21.7	30.80	32.10	27.9	17.2	20.6	27.5	23.6
Sm	4.65	4.07	5.91	5.45	4.63	3.17	4.29	5.07	4.97
Eu	0.75	0.61	0.85	0.85	0.55	0.56	0.55	0.64	0.66
Gd	4.00	3.46	5.83	4.66	4.27	3.03	4.24	4.80	4.93
Tb	0.77	0.72	1.02	0.95	0.66	0.47	0.71	0.79	0.83
Dy	4.74	4.24	6.72	5.43	4.19	2.91	4.61	5.17	5.52
Ho	0.95	0.92	1.36	1.21	0.87	0.62	1.01	1.09	1.19
Er	3.21	3.13	4.50	3.56	2.84	1.95	3.25	3.51	3.88

Tm	0.53	0.53	0.83	0.62	0.44	0.31	0.52	0.55	0.63
Yb	3.84	3.98	5.64	4.69	3.15	2.11	3.85	3.89	4.41
Lu	0.63	0.65	0.91	0.68	0.49	0.34	0.60	0.60	0.69
$\Sigma$ REE	191	146	218	233	181	110	127	176	145
LREE/ HREE	9.22	7.27	7.15	9.68	9.73	8.41	5.76	7.62	5.55
Eu/Eu*	0.52	0.48	0.44	0.50	0.37	0.54	0.39	0.39	0.40
(La/Sm) <sub>N</sub>	6.09	4.96	5.27	6.53	5.94	5.13	3.87	4.93	3.75
Trace element (ppm)									
Rb	236	240	214	231	244	236	259	246	280
Ba	389	386	380	455	218	416	286	304	302
Th	29.8	31.2	35.8	34.6	35.6	27.8	33.5	38.4	40.0
U	6.16	8.8	8.21	5.72	3.57	3.38	4.02	4.2	4.92
Nb	18.5	20.6	22.7	17.6	13.4	9.45	15.4	15.8	18.2
Ta	3.08	3.16	4.98	2.63	1.88	1.1	1.81	2.08	2.47
Sr	207	206	200	199	108	163	121	122	122
Zr	146	114	127	117	69.5	73.6	82.5	89.3	113
Hf	5.33	4.03	4.95	4.39	3.03	3.1	3.56	3.85	4.86
Y	29.7	29.1	39.1	33.7	25.4	17.6	29.1	30.8	34.5
Ni	7.35	6.64	7.42	7.48	1.33	1.39	1.41	1.58	1.59
Sc	7.04	8.11	8.65	8.84	4.41	4.53	4.1	4.93	5.5

Table 2

Spot No.	Pb	Th	U	Th/U	$^{207}\text{Pb}/^{206}\text{Pb}$	$^{207}\text{Pb}/^{235}\text{U}$	$^{206}\text{Pb}/^{238}\text{U}$	age (Ma)
	ppm	U	$^{206}\text{Pb}$	$1\sigma$	$^{238}\text{U}$	$1\sigma$	$^{206}\text{Pb}/^{238}\text{U}$	$1\sigma$
<b>15QLP-9(<math>\delta_1</math>)</b>								
1	141	1542	1420	1.1	0.04902	0.00272	0.12501	0.00659
2	228	2678	2421	1.1	0.05095	0.00223	0.12508	0.00548
3	137	279	1459	0.2	0.06204	0.00202	0.51179	0.01648
4	38	252	701	0.4	0.04857	0.00298	0.13015	0.00772
5	57	520	1121	0.5	0.04980	0.00468	0.11756	0.01109
6	32	251	847	0.3	0.05151	0.00437	0.12592	0.00987
7	147	1518	1176	1.3	0.05049	0.00358	0.13863	0.00966
8	139	1402	1826	0.8	0.05146	0.00236	0.13652	0.00634
9	261	3148	2287	1.4	0.04747	0.00170	0.11757	0.00444
10	183	2116	1758	1.2	0.04807	0.00205	0.12200	0.00558
11	902	11300	5444	2.1	0.04778	0.00132	0.11803	0.00343
12	620	8008	4217	1.9	0.04808	0.00144	0.11756	0.00368
13	314	3515	2359	1.5	0.05033	0.00198	0.13171	0.00515
14	484	5785	3314	1.7	0.04804	0.00172	0.12419	0.00442
15	188	1988	2193	0.9	0.04750	0.00202	0.12330	0.00539
16	341	3948	2930	1.3	0.05106	0.00190	0.12625	0.00438
17	279	3063	2215	1.4	0.04721	0.00188	0.12405	0.00515
18	569	6822	3450	2.0	0.04796	0.00155	0.12054	0.00391
19	618	7418	4104	1.8	0.04849	0.00180	0.13053	0.00542
20	110	1060	1255	0.8	0.04950	0.00246	0.12911	0.00633
21	147	1529	1346	1.1	0.04821	0.00255	0.13446	0.00738
22	25	193	521	0.4	0.05605	0.00565	0.13423	0.01242
<b>15QML-65 (<math>\delta_2</math>)</b>								
1	23	246	178	1.4	0.13903	0.01718	0.31150	0.03046
2	42	419	328	1.3	0.08319	0.00610	0.24530	0.02157
3	42	438	262	1.7	0.10495	0.01279	0.22321	0.01690
4	97	969	545	1.8	0.05175	0.00370	0.13438	0.00961
5	117	1316	761	1.7	0.05293	0.00396	0.13010	0.00906
6	162	1619	781	2.1	0.05584	0.00332	0.15124	0.00907
7	287	3022	1342	2.3	0.04963	0.00249	0.12762	0.00605
8	95	1061	579	1.8	0.05587	0.00530	0.13131	0.01217
9	74	718	590	1.2	0.06569	0.00424	0.16535	0.01032
10	282	2897	1274	2.3	0.05469	0.00290	0.14266	0.00717
11	89	894	551	1.6	0.06789	0.00457	0.17148	0.01149
12	49	549	319	1.7	0.07802	0.00620	0.19621	0.01456
13	34	351	311	1.1	0.06224	0.00661	0.14623	0.01464
14	47	511	325	1.6	0.08325	0.00723	0.19478	0.01501
							0.01857	0.00042
							0.01857	0.00042

15	128	1404	807	1.7	0.05491	0.00371	0.13408	0.00869	0.01816	0.00029	116	1.8
16	92	997	576	1.7	0.05330	0.00431	0.13535	0.01059	0.01875	0.00040	120	2.5
17	169	1656	832	2.0	0.05248	0.00451	0.13911	0.01149	0.01982	0.00040	127	2.5
18	221	2432	1054	2.3	0.04855	0.00301	0.12207	0.00726	0.01838	0.00027	117	1.7
19	76	782	602	1.3	0.05473	0.00429	0.13385	0.00963	0.01847	0.00033	118	2.1
20	87	867	485	1.8	0.08114	0.00558	0.21182	0.01376	0.01967	0.00035	126	2.2
<b>15QMH-1 (<math>\gamma\delta_1</math>)</b>												
1	49	504	407	1.2	0.04914	0.00280	0.12710	0.00696	0.01903	0.00030	122	1.9
2	20	193	219	0.9	0.06130	0.00353	0.15841	0.00896	0.01917	0.00034	122	2.1
3	26	220	520	0.4	0.05303	0.00342	0.13768	0.00900	0.01883	0.00031	120	1.9
4	67	620	590	1.1	0.05015	0.00230	0.13691	0.00615	0.01987	0.00027	127	1.7
5	62	617	626	1.0	0.04896	0.00219	0.13040	0.00578	0.01923	0.00023	123	1.4
6	36	362	397	0.9	0.04876	0.00276	0.12348	0.00697	0.01831	0.00025	117	1.6
7	16	147	218	0.7	0.05490	0.00507	0.13727	0.01078	0.01915	0.00036	122	2.3
8	42	445	470	0.9	0.04816	0.00263	0.12775	0.00652	0.01913	0.00028	122	1.8
9	22	180	259	0.7	0.06290	0.00424	0.16174	0.01041	0.01863	0.00034	119	2.1
10	31	320	338	0.9	0.04673	0.00380	0.11830	0.00780	0.01911	0.00028	122	1.8
11	87	815	826	1.0	0.04580	0.00197	0.12634	0.00466	0.01968	0.00024	126	1.5
12	16	158	185	0.9	0.04735	0.00377	0.12959	0.01005	0.01990	0.00037	127	2.3
13	29	260	278	0.9	0.05051	0.00360	0.13024	0.00822	0.01964	0.00035	125	2.2
14	22	193	250	0.8	0.05610	0.00420	0.15242	0.01020	0.02052	0.00035	131	2.2
15	34	319	347	0.9	0.05417	0.00337	0.14257	0.00821	0.01975	0.00032	126	2.0
16	35	354	375	0.9	0.04909	0.00294	0.12539	0.00705	0.01876	0.00026	120	1.7
17	40	412	379	1.1	0.05066	0.00302	0.13020	0.00760	0.01861	0.00028	119	1.8
18	25	250	282	0.9	0.05207	0.00439	0.12989	0.01031	0.01848	0.00040	118	2.5
19	27	259	277	0.9	0.05488	0.00360	0.14768	0.00974	0.01952	0.00031	125	1.9
20	21	207	241	0.9	0.05534	0.00447	0.12923	0.00961	0.01754	0.00041	112	2.6
21	23	217	339	0.6	0.05525	0.00343	0.13480	0.00825	0.01804	0.00030	115	1.9
22	41	365	323	1.1	0.05184	0.00287	0.14069	0.00736	0.02008	0.00032	128	2.0
<b>15QLL-21(<math>\gamma\delta_2</math>)</b>												
1	226	1501	3249	0.5	0.05066	0.00212	0.14002	0.00574	0.02026	0.00033	129	2.1
2	114	881	1322	0.7	0.05362	0.00265	0.14635	0.00699	0.02035	0.00040	130	2.5
3	149	1158	1298	0.9	0.05212	0.00289	0.13834	0.00777	0.01961	0.00039	125	2.5
4	111	856	1225	0.7	0.05146	0.00261	0.14954	0.00757	0.02116	0.00032	135	2.0
5	142	1066	1343	0.8	0.05225	0.00259	0.14999	0.00724	0.02113	0.00033	135	2.1
6	141	1011	1914	0.5	0.04883	0.00209	0.13630	0.00587	0.02063	0.00038	132	2.4
7	197	1536	1921	0.8	0.04780	0.00205	0.13164	0.00573	0.02015	0.00033	129	2.1
8	382	2956	5414	0.5	0.05047	0.00155	0.13237	0.00409	0.01912	0.00030	122	1.9
9	106	813	957	0.8	0.05454	0.00295	0.15680	0.00865	0.02092	0.00031	133	2.0
10	256	1817	4444	0.4	0.04958	0.00155	0.13828	0.00423	0.02030	0.00029	130	1.8
11	75	573	962	0.6	0.05177	0.00317	0.14141	0.00844	0.02028	0.00033	129	2.1
12	234	2153	3395	0.6	0.04900	0.00166	0.13014	0.00489	0.01915	0.00028	122	1.8
13	83	649	850	0.8	0.05222	0.00341	0.13972	0.00867	0.01993	0.00036	127	2.3
14	88	706	1413	0.5	0.05120	0.00270	0.12283	0.00612	0.01789	0.00032	114	2.0

15	135	1110	1560	0.7	0.05048	0.00231	0.14107	0.00648	0.02041	0.00030	130	1.9
16	108	928	1247	0.7	0.04778	0.00269	0.12215	0.00676	0.01886	0.00035	120	2.2
17	120	1019	1155	0.9	0.05280	0.00274	0.14031	0.00720	0.01948	0.00036	124	2.3
18	58	470	702	0.7	0.05197	0.00319	0.14206	0.00883	0.02002	0.00032	128	2.0
19	34	237	561	0.4	0.05569	0.00373	0.16935	0.01107	0.02259	0.00049	144	3.1
20	158	1288	1749	0.7	0.04830	0.00188	0.13376	0.00571	0.01995	0.00025	127	1.6
21	183	1381	1186	1.2	0.05429	0.00283	0.15200	0.00789	0.02044	0.00036	130	2.3
22	119	913	1574	0.6	0.04812	0.00232	0.12876	0.00642	0.01942	0.00033	124	2.1

15QML-57 ( $\gamma\delta_3$ )

1	30	243	318	0.8	0.08319	0.01147	0.20507	0.02163	0.01949	0.00052	124	3.3
2	212	1933	2410	0.8	0.04995	0.00185	0.13817	0.00514	0.01999	0.00022	128	1.4
3	45	417	350	1.2	0.06965	0.00715	0.17504	0.01619	0.01918	0.00060	122	3.8
4	90	931	759	1.2	0.05363	0.00350	0.13775	0.00861	0.01893	0.00036	121	2.3
5	42	426	505	0.8	0.05884	0.00518	0.14526	0.01165	0.01913	0.00051	122	3.2
6	66	645	624	1.0	0.05668	0.00360	0.14738	0.00884	0.01939	0.00032	124	2.0
7	52	475	343	1.4	0.07539	0.00795	0.20314	0.01895	0.02052	0.00056	131	3.6
8	47	456	511	0.9	0.06336	0.00510	0.16027	0.01306	0.01888	0.00039	121	2.5
9	74	777	718	1.1	0.05620	0.00509	0.14233	0.01261	0.01855	0.00035	118	2.2
10	126	1297	960	1.4	0.05468	0.00412	0.14273	0.01093	0.01928	0.00027	123	1.7
11	48	446	512	0.9	0.05712	0.00758	0.13425	0.01564	0.01807	0.00042	115	2.7
12	90	934	834	1.1	0.05265	0.00307	0.13279	0.00756	0.01877	0.00032	120	2.0
13	36	353	444	0.8	0.06705	0.00518	0.16900	0.01301	0.01850	0.00034	118	2.2
14	65	612	716	0.9	0.04651	0.00319	0.12036	0.00839	0.01888	0.00033	121	2.1
15	71	705	719	1.0	0.05376	0.00348	0.14240	0.00904	0.01936	0.00027	124	1.7
16	79	788	707	1.1	0.04967	0.00339	0.12764	0.00901	0.01850	0.00034	118	2.1
17	53	525	609	0.9	0.05007	0.00427	0.12193	0.01021	0.01827	0.00029	117	1.8
18	32	293	371	0.8	0.06998	0.00557	0.18318	0.01384	0.01912	0.00040	122	2.5
19	32	307	446	0.7	0.04913	0.00398	0.12461	0.00989	0.01871	0.00032	120	2.0
20	55	501	489	1.0	0.05697	0.00485	0.14265	0.01116	0.01938	0.00038	124	2.4

10QTG-42( $\gamma_1$ )

1	64	1385	2646	0.5	0.04933	0.00130	0.13383	0.00366	0.01950	0.00018	124	1.1
2	16	375	656	0.6	0.04910	0.00165	0.12961	0.00433	0.01904	0.00018	122	1.1
3	30	828	1234	0.7	0.04830	0.00166	0.12632	0.00412	0.01893	0.00019	121	1.2
4	7	204	265	0.8	0.05261	0.00279	0.13574	0.00728	0.01874	0.00026	120	1.6
5	6	140	228	0.6	0.05338	0.00271	0.13712	0.00668	0.01881	0.00028	120	1.8
6	10	773	298	2.6	0.04712	0.00420	0.11410	0.00976	0.01790	0.00032	114	2.0
7	20	696	689	1.0	0.05401	0.00248	0.14662	0.00662	0.01964	0.00021	125	1.3
8	22	606	825	0.7	0.04933	0.00154	0.14056	0.00445	0.02065	0.00026	132	1.6
9	14	609	563	1.1	0.05338	0.00218	0.13141	0.00526	0.01790	0.00018	114	1.1
10	10	334	370	0.9	0.05759	0.00294	0.14801	0.00713	0.01883	0.00023	120	1.4
11	14	620	512	1.2	0.05209	0.00262	0.13746	0.00690	0.01903	0.00020	122	1.3
12	13	485	509	1.0	0.05284	0.00188	0.13343	0.00464	0.01839	0.00018	117	1.1
13	10	389	362	1.1	0.04649	0.00205	0.12270	0.00524	0.01931	0.00022	123	1.4
14	18	617	680	0.9	0.05522	0.00226	0.15049	0.00647	0.01955	0.00022	125	1.4

15	19	599	672	0.9	0.05222	0.00189	0.15046	0.00555	0.02086	0.00026	133	1.6
16	33	1098	1232	0.9	0.05292	0.00152	0.14469	0.00426	0.01974	0.00018	126	1.1
17	11	349	426	0.8	0.05121	0.00209	0.13135	0.00536	0.01859	0.00021	119	1.3
18	6	250	236	1.1	0.05259	0.00381	0.12887	0.00935	0.01779	0.00031	114	2.0
19	14	570	532	1.1	0.05016	0.00212	0.12503	0.00518	0.01805	0.00020	115	1.2
20	19	504	719	0.7	0.04937	0.00175	0.14321	0.00522	0.02095	0.00020	134	1.3

15QML-5( $\gamma_2$ )

1	78	547	733	0.7	0.05568	0.00347	0.15320	0.00914	0.02066	0.00046	132	2.9
2	71	437	722	0.6	0.04919	0.00365	0.14398	0.01089	0.02105	0.00047	134	2.9
3	99	680	1025	0.7	0.05592	0.00296	0.15595	0.00825	0.02046	0.00037	131	2.3
4	104	680	1588	0.4	0.05017	0.00308	0.13490	0.00769	0.01987	0.00037	127	2.3
5	973	7982	5413	1.5	0.04971	0.00176	0.12889	0.00414	0.01909	0.00035	122	2.2
6	76	425	1222	0.3	0.05063	0.00313	0.13793	0.00823	0.02036	0.00043	130	2.7
7	73	477	625	0.8	0.04940	0.00383	0.13537	0.01009	0.02028	0.00044	129	2.8
8	111	673	1163	0.6	0.04995	0.00305	0.13752	0.00865	0.02069	0.00058	132	3.7
9	63	444	767	0.6	0.05471	0.00389	0.14188	0.00957	0.01926	0.00045	123	2.9
10	265	1983	1351	1.5	0.05045	0.00247	0.13700	0.00675	0.01977	0.00038	126	2.4
11	195	1277	3005	0.4	0.04902	0.00195	0.14695	0.00596	0.02166	0.00037	138	2.3
12	95	624	1054	0.6	0.05697	0.00377	0.15132	0.00881	0.02005	0.00046	128	2.9
13	54	360	486	0.7	0.06170	0.00808	0.16407	0.02093	0.01977	0.00062	126	3.9
14	159	1305	1156	1.1	0.05017	0.00291	0.13377	0.00728	0.01971	0.00032	126	2.0
15	274	1950	2894	0.7	0.05417	0.00216	0.15823	0.00663	0.02088	0.00033	133	2.1
16	100	763	862	0.9	0.05454	0.00343	0.14874	0.00858	0.02065	0.00039	132	2.5
17	178	1443	1298	1.1	0.05180	0.00274	0.14138	0.00724	0.01992	0.00026	127	1.7
18	78	547	1043	0.5	0.05423	0.00291	0.14625	0.00727	0.02005	0.00032	128	2.0
19	205	1712	2211	0.8	0.05003	0.00201	0.13206	0.00521	0.01919	0.00022	123	1.4
20	111	942	1089	0.9	0.04923	0.00293	0.13277	0.00767	0.01966	0.00029	126	1.8
21	164	1421	1276	1.1	0.05365	0.00289	0.14390	0.00755	0.01963	0.00028	125	1.8
22	56	479	543	0.9	0.06584	0.00611	0.15846	0.01260	0.01908	0.00047	122	2.9
23	72	609	656	0.9	0.05762	0.00583	0.15799	0.01446	0.02116	0.00058	135	3.7
24	81	661	889	0.7	0.05702	0.00477	0.14416	0.01189	0.01900	0.00039	121	2.5
25	85	760	770	1.0	0.04898	0.00319	0.13222	0.00867	0.01973	0.00033	126	2.1
26	98	762	850	0.9	0.05038	0.00338	0.14511	0.00904	0.02157	0.00033	138	2.1

15QML-83 ( $\gamma_3$ )

1	179	1790	3085	0.6	0.04733	0.00109	0.11207	0.00268	0.01703	0.00018	109	1.1
2	152	1709	1486	1.1	0.04771	0.00141	0.12197	0.00371	0.01844	0.00021	118	1.3
3	222	2372	3602	0.7	0.04735	0.00102	0.11333	0.00256	0.01722	0.00016	110	1.0
4	310	3868	2685	1.4	0.04647	0.00117	0.10844	0.00275	0.01683	0.00015	108	0.9
5	170	1693	2677	0.6	0.04685	0.00119	0.11344	0.00296	0.01748	0.00018	112	1.1
6	122	1177	2764	0.4	0.04814	0.00123	0.11196	0.00287	0.01681	0.00017	107	1.1
7	75	783	1262	0.6	0.04725	0.00158	0.11915	0.00407	0.01821	0.00023	116	1.5
8	82	847	1524	0.6	0.04924	0.00155	0.12399	0.00402	0.01825	0.00022	117	1.4
9	134	1219	2315	0.5	0.04714	0.00123	0.11298	0.00287	0.01731	0.00015	111	1.0
10	203	2452	2729	0.9	0.04599	0.00113	0.10633	0.00263	0.01668	0.00016	107	1.0

11	222	2468	4376	0.6	0.04695	0.00103	0.10957	0.00235	0.01683	0.00014	108	0.9
12	254	2914	3379	0.9	0.04643	0.00108	0.11074	0.00261	0.01719	0.00017	110	1.1
13	74	829	1201	0.7	0.04813	0.00150	0.11600	0.00344	0.01747	0.00018	112	1.1
14	176	1591	4696	0.3	0.04808	0.00120	0.11766	0.00300	0.01761	0.00020	113	1.2
15	76	692	1856	0.4	0.04773	0.00146	0.12080	0.00380	0.01821	0.00022	116	1.4
16	32	76.4	1104	0.1	0.04973	0.00143	0.20831	0.00582	0.03023	0.00032	192	2.0
17	230	2502	4989	0.5	0.04525	0.00099	0.10648	0.00228	0.01692	0.00014	108	0.9
18	72	729	1208	0.6	0.04784	0.00162	0.11964	0.00406	0.01807	0.00019	115	1.2
19	111	1038	2737	0.4	0.04665	0.00122	0.11153	0.00290	0.01721	0.00015	110	0.9
20	162	417	635	0.7	0.05633	0.00142	0.48045	0.01611	0.06084	0.00135	381	8.2
<b>15QLR-4(<math>\gamma_4</math>)</b>												
1	116	1214	1165	1.0	0.04965	0.00270	0.12570	0.00671	0.01851	0.00025	118	1.6
2	86	874	1064	0.8	0.05360	0.00261	0.13316	0.00655	0.01818	0.00030	116	1.9
3	185	1880	2175	0.9	0.04615	0.00171	0.12879	0.00493	0.02024	0.00032	129	2.0
4	85	897	1180	0.8	0.04931	0.00260	0.12217	0.00620	0.01812	0.00022	116	1.4
5	193	1904	1560	1.2	0.05091	0.00242	0.13755	0.00642	0.01959	0.00021	125	1.3
6	103	1078	1196	0.9	0.04991	0.00239	0.12304	0.00562	0.01795	0.00021	115	1.3
7	21	190	4550	0.0	0.04881	0.00263	0.03135	0.00154	0.00478	0.00008	31	0.5
8	195	2255	1738	1.3	0.04792	0.00215	0.12000	0.00520	0.01821	0.00023	116	1.5
9	168	1755	4242	0.4	0.04788	0.00185	0.07982	0.00350	0.01185	0.00024	76	1.5
10	49	500	831	0.6	0.04705	0.00303	0.12009	0.00757	0.01874	0.00028	120	1.8
11	190	1894	2421	0.8	0.05204	0.00184	0.14750	0.00555	0.02046	0.00032	131	2.0
12	90	886	937	0.9	0.05226	0.00267	0.13854	0.00657	0.01959	0.00029	125	1.8
13	117	1164	1268	0.9	0.05221	0.00262	0.13404	0.00669	0.01848	0.00023	118	1.4
14	110	1102	1331	0.8	0.05286	0.00244	0.13797	0.00633	0.01900	0.00026	121	1.6
15	355	4382	2070	2.1	0.05257	0.00217	0.13106	0.00520	0.01811	0.00020	116	1.3
16	126	1326	1264	1.0	0.04827	0.00263	0.12323	0.00676	0.01853	0.00026	118	1.6
17	51	435	3983	0.1	0.04906	0.00338	0.03782	0.00259	0.00556	0.00010	36	0.6
18	68	707	800	0.9	0.05059	0.00327	0.12812	0.00844	0.01872	0.00029	120	1.8
19	96	951	1068	0.9	0.05383	0.00273	0.14073	0.00723	0.01887	0.00024	121	1.5
20	107	1187	1281	0.9	0.04918	0.00223	0.11356	0.00544	0.01675	0.00032	107	2.0
21	103	1055	1059	1.0	0.05304	0.00283	0.14531	0.00845	0.01954	0.00033	125	2.1
22	126	1395	1138	1.2	0.04989	0.00251	0.12120	0.00597	0.01765	0.00021	113	1.3
23	224	1990	1163 6	0.2	0.04793	0.00129	0.06714	0.00187	0.01014	0.00012	65	0.8
24	129	1361	1066	1.3	0.05039	0.00274	0.13085	0.00670	0.01932	0.00034	123	2.1
25	124	1306	1339	1.0	0.05039	0.00235	0.12765	0.00568	0.01861	0.00022	119	1.4
26	82	723	601	1.2	0.05503	0.00618	0.15003	0.01513	0.02131	0.00058	136	3.7
<b>15QLM-37(<math>\gamma_5</math>)</b>												
1	99	885	1297	0.7	0.0480	0.0025	0.1284	0.0065	0.0197	0.0003	126	1.8
2	72	597	1110	0.5	0.0520	0.0026	0.1369	0.0068	0.0191	0.0003	122	1.7
3	125	1190	1482	0.8	0.0496	0.0024	0.1308	0.0063	0.0192	0.0002	122	1.5
4	166	1723	1139	1.5	0.0460	0.0027	0.1206	0.0068	0.0191	0.0003	122	2
5	133	1253	2019	0.6	0.0483	0.0021	0.1207	0.0053	0.0180	0.0002	115	1.3

6	181	1656	1860	0.9	0.0502	0.0020	0.1366	0.0051	0.0200	0.0003	128	1.6
7	150	1493	1363	1.1	0.0496	0.0026	0.1320	0.0070	0.0193	0.0003	123	1.9
8	143	886	1045	0.8	0.0828	0.0056	0.2461	0.0178	0.0214	0.0003	137	1.8
9	216	2444	1664	1.5	0.0523	0.0028	0.1312	0.0070	0.0183	0.0002	117	1.4
10	66.0	668	905	0.7	0.0542	0.0038	0.1297	0.0088	0.0174	0.0003	111	1.7
11	27.8	258	317	0.8	0.0856	0.0070	0.2258	0.0179	0.0200	0.0005	128	3.1
12	88	847	969	0.9	0.0483	0.0029	0.1301	0.0083	0.0196	0.0003	125	1.9
13	126	1167	1483	0.8	0.0461	0.0026	0.1213	0.0066	0.0193	0.0002	123	1.5
14	241	2277	2837	0.8	0.0502	0.0017	0.1298	0.0044	0.0186	0.0002	119	1.2
15	51.1	339	683	0.5	0.0561	0.0051	0.1485	0.0113	0.0202	0.0003	129	2.2
16	127	1268	1419	0.9	0.0489	0.0024	0.1241	0.0060	0.0187	0.0002	120	1.5
17	119	1022	1315	0.8	0.0538	0.0024	0.1534	0.0069	0.0208	0.0003	132	1.7
18	126	1287	871	1.5	0.0538	0.0040	0.1329	0.0098	0.0180	0.0003	115	2.1
19	277	3043	1371	2.2	0.0495	0.0025	0.1291	0.0065	0.0191	0.0003	122	1.7
20	166	1310	2822	0.5	0.0481	0.0019	0.1255	0.0050	0.0189	0.0002	121	1.2
21	83	804	989	0.8	0.0539	0.0047	0.1324	0.0110	0.0182	0.0003	117	2.1
22	77	695	1078	0.6	0.0464	0.0026	0.1200	0.0066	0.0189	0.0003	121	1.6

ACCEPTED MANUSCRIPT

Table 3

Spot No.	$^{176}\text{Hf}/^{177}\text{Hf}$	1σ	$^{176}\text{Lu}/^{177}\text{Hf}$	1σ	$^{176}\text{Yb}/^{177}\text{Hf}$	1σ	$\epsilon\text{Hf(t)}$	1σ	$T_{\text{DM}}$	$T_{\text{DM}}^{\text{c}}$
<b>15QML-65</b>										
4	0.28279	0.00003	0.00130	0.00001	0.04782	0.00037	3.1	1.1	664	873
5	0.28279	0.00003	0.00127	0.00001	0.04372	0.00032	3.1	1.1	661	869
6	0.28279	0.00003	0.00194	0.00002	0.06754	0.00052	3.1	1.3	674	874
7	0.28280	0.00003	0.00188	0.00002	0.06013	0.00051	3.3	1.2	662	858
8	0.28279	0.00002	0.00128	0.00002	0.03827	0.00058	3.1	0.9	663	871
9	0.28283	0.00003	0.00107	0.00000	0.03619	0.00027	4.6	1.3	599	787
10	0.28280	0.00003	0.00204	0.00002	0.06465	0.00126	3.6	1.2	655	845
11	0.28282	0.00002	0.00112	0.00003	0.03456	0.00091	4.2	1.0	617	811
12	0.28285	0.00003	0.00092	0.00002	0.03367	0.00108	5.4	1.0	567	744
13	0.28284	0.00005	0.00113	0.00002	0.03983	0.00066	5.0	1.8	584	766
14	0.28299	0.00004	0.00076	0.00002	0.02738	0.00071	10.3	1.5	367	467
15	0.28281	0.00002	0.00212	0.00005	0.07700	0.00207	3.9	1.0	641	825
16	0.28285	0.00002	0.00112	0.00000	0.03589	0.00030	5.3	1.0	573	750
17	0.28284	0.00002	0.00176	0.00002	0.06403	0.00075	4.9	0.9	596	771
18	0.28273	0.00006	0.00160	0.00001	0.06234	0.00066	1.2	2.2	746	979
19	0.28277	0.00003	0.00102	0.00001	0.03556	0.00031	2.4	1.0	686	909
20	0.28276	0.00003	0.00126	0.00002	0.04758	0.00094	2.1	1.0	703	928
<b>15QMH-1</b>										
1	0.28261	0.00002	0.00129	0.00001	0.04492	0.00114	-3.4	0.8	920	1229
2	0.28266	0.00002	0.00080	0.00002	0.02417	0.00038	-1.5	0.8	834	1122
3	0.28264	0.00002	0.00090	0.00002	0.02718	0.00082	-2.2	0.8	865	1163
4	0.28260	0.00002	0.00125	0.00003	0.03664	0.00072	-3.5	0.9	925	1237
5	0.28255	0.00003	0.00120	0.00002	0.03600	0.00055	-5.2	1.0	992	1331
6	0.28267	0.00002	0.00172	0.00002	0.05529	0.00060	-1.1	0.8	836	1101
7	0.28243	0.00002	0.00104	0.00001	0.02898	0.00035	-9.4	1.0	1156	1564
8	0.28257	0.00002	0.00110	0.00002	0.02903	0.00050	-4.5	1.0	965	1295
9	0.28254	0.00001	0.00063	0.00002	0.02199	0.00091	-5.7	0.7	1000	1359
10	0.28252	0.00002	0.00105	0.00001	0.02941	0.00136	-6.4	0.8	1039	1399
11	0.28246	0.00002	0.00123	0.00002	0.04220	0.00082	-8.4	0.8	1124	1512
12	0.28271	0.00002	0.00070	0.00000	0.02202	0.00030	0.2	0.8	768	1031
13	0.28253	0.00003	0.00089	0.00001	0.02780	0.00066	-5.8	1.1	1012	1367
14	0.28254	0.00002	0.00084	0.00001	0.02458	0.00030	-5.7	0.9	1004	1358
15	0.28260	0.00002	0.00132	0.00002	0.04922	0.00136	-3.6	0.8	932	1242
16	0.28261	0.00002	0.00144	0.00001	0.04640	0.00063	-3.3	0.9	926	1230
17	0.28248	0.00002	0.00136	0.00001	0.04188	0.00040	-7.9	0.9	1108	1484
18	0.28257	0.00002	0.00086	0.00003	0.02269	0.00065	-4.6	0.8	963	1300
19	0.28255	0.00003	0.00120	0.00003	0.03529	0.00097	-5.1	1.2	992	1330
20	0.28245	0.00002	0.00091	0.00002	0.02770	0.00041	-8.7	0.9	1126	1526

21	0.28253	0.00003	0.00100	0.00002	0.02586	0.00061	-5.8	1.1	1015	1368
22	0.28242	0.00007	0.00194	0.00003	0.04996	0.00356	-9.8	2.5	1200	1588

## 15QLL-21

1	0.28260	0.00002	0.00133	0.00001	0.04764	0.00047	-3.5	0.8	934	1243
2	0.28258	0.00002	0.00098	0.00000	0.03395	0.00034	-4.2	0.9	957	1285
3	0.28261	0.00002	0.00131	0.00004	0.04599	0.00156	-3.1	0.8	921	1225
4	0.28256	0.00002	0.00092	0.00001	0.03380	0.00035	-4.7	0.8	976	1313
5	0.28278	0.00006	0.00143	0.00003	0.05354	0.00239	2.9	2.2	679	888
6	0.28250	0.00002	0.00135	0.00004	0.04738	0.00174	-6.9	0.9	1072	1433
7	0.28257	0.00002	0.00163	0.00002	0.05931	0.00102	-4.5	0.8	981	1298
8	0.28253	0.00002	0.00093	0.00001	0.03228	0.00024	-5.7	0.9	1015	1368
9	0.28257	0.00002	0.00160	0.00002	0.05539	0.00066	-4.3	0.8	975	1291
10	0.28255	0.00002	0.00098	0.00001	0.03362	0.00036	-5.3	0.8	998	1343
11	0.28258	0.00002	0.00101	0.00001	0.03386	0.00039	-4.1	0.8	951	1276
12	0.28264	0.00002	0.00082	0.00000	0.02747	0.00029	-1.9	0.9	861	1155
13	0.28260	0.00002	0.00121	0.00004	0.04082	0.00111	-3.4	1.0	927	1237
14	0.28256	0.00002	0.00105	0.00002	0.03537	0.00065	-4.7	0.9	978	1313
15	0.28260	0.00002	0.00159	0.00003	0.05260	0.00058	-3.4	0.9	939	1241
16	0.28260	0.00002	0.00061	0.00001	0.02092	0.00060	-3.2	0.8	910	1230
17	0.28259	0.00002	0.00167	0.00002	0.06025	0.00041	-3.8	0.8	954	1260
18	0.28282	0.00010	0.00145	0.00004	0.05534	0.00346	4.4	3.7	620	807

## 15QML-57

2	0.28277	0.00003	0.00122	0.00003	0.03360	0.00081	2.7	1.2	680	896
3	0.28272	0.00004	0.00097	0.00007	0.03569	0.00229	0.8	1.5	752	1001
4	0.28265	0.00003	0.00073	0.00002	0.02360	0.00092	-1.9	1.0	853	1150
5	0.28263	0.00004	0.00077	0.00002	0.02290	0.00062	-2.3	1.4	871	1173
6	0.28266	0.00003	0.00158	0.00001	0.04587	0.00030	-1.6	1.1	858	1132
7	0.28265	0.00003	0.00049	0.00001	0.01405	0.00040	-1.5	1.2	835	1130
8	0.28261	0.00004	0.00236	0.00005	0.07374	0.00188	-3.3	1.4	946	1230
9	0.28267	0.00006	0.00132	0.00001	0.04240	0.00129	-1.1	2.0	834	1106
10	0.28273	0.00005	0.00110	0.00001	0.03694	0.00079	1.1	1.7	743	986
11	0.28266	0.00024	0.00229	0.00002	0.07209	0.00078	-1.6	8.4	875	1136
12	0.28267	0.00002	0.00088	0.00000	0.02781	0.00029	-1.0	1.0	821	1100
13	0.28270	0.00002	0.00121	0.00005	0.03836	0.00233	-0.1	0.9	790	1049
14	0.28262	0.00001	0.00157	0.00001	0.04944	0.00025	-3.0	0.7	916	1212
15	0.28270	0.00003	0.00151	0.00001	0.04641	0.00090	0.1	1.3	790	1041
16	0.28268	0.00002	0.00102	0.00002	0.03239	0.00101	-0.5	1.0	805	1074
17	0.28266	0.00005	0.00180	0.00002	0.05475	0.00123	-1.5	1.8	861	1131

## 10QTG-42

1	0.28260	0.00002	0.00224	0.00003	0.06927	0.00106	-3.6	0.8	952	1243
2	0.28258	0.00001	0.00146	0.00001	0.04359	0.00025	-4.2	0.7	956	1273
3	0.28258	0.00002	0.00158	0.00001	0.04637	0.00046	-4.2	0.8	960	1275
6	0.28263	0.00002	0.00092	0.00005	0.03121	0.00208	-2.4	0.9	875	1177
7	0.28259	0.00002	0.00140	0.00001	0.04494	0.00042	-3.9	0.8	945	1260

8	0.28262	0.00001	0.00135	0.00001	0.03842	0.00042	-3.0	0.7	907	1209
9	0.28255	0.00002	0.00112	0.00001	0.03355	0.00037	-5.4	0.8	999	1344
10	0.28258	0.00002	0.00108	0.00000	0.03376	0.00025	-4.3	0.9	952	1279
11	0.28264	0.00002	0.00128	0.00001	0.04153	0.00050	-2.3	0.8	878	1170
12	0.28257	0.00002	0.00099	0.00001	0.03378	0.00075	-4.5	0.8	959	1292
13	0.28262	0.00001	0.00101	0.00001	0.03291	0.00058	-2.7	0.7	889	1193
14	0.28267	0.00002	0.00128	0.00001	0.04133	0.00030	-1.1	0.8	828	1101
15	0.28260	0.00002	0.00231	0.00005	0.06248	0.00079	-3.6	0.8	952	1241
16	0.28261	0.00002	0.00190	0.00007	0.05182	0.00163	-3.3	0.8	929	1222
17	0.28259	0.00002	0.00123	0.00001	0.03729	0.00039	-4.0	0.8	946	1266
18	0.28253	0.00001	0.00079	0.00001	0.02564	0.00018	-6.0	0.7	1013	1374
19	0.28259	0.00002	0.00129	0.00001	0.04131	0.00052	-3.9	0.8	941	1258
20	0.28256	0.00001	0.00142	0.00001	0.04460	0.00047	-5.1	0.7	992	1324

## 15QML-83

1	0.28260	0.00003	0.00254	0.00004	0.09195	0.00251	-3.6	1.1	958	1242
2	0.28260	0.00002	0.00236	0.00004	0.07995	0.00124	-3.8	1.0	962	1253
3	0.28261	0.00002	0.00228	0.00003	0.08389	0.00196	-3.2	1.0	937	1221
4	0.28260	0.00002	0.00246	0.00006	0.08820	0.00165	-3.8	1.0	966	1254
5	0.28263	0.00003	0.00241	0.00004	0.07640	0.00109	-2.6	1.2	913	1185
6	0.28267	0.00002	0.00220	0.00003	0.06875	0.00104	-1.1	0.8	847	1103
7	0.28263	0.00003	0.00205	0.00002	0.07014	0.00053	-2.5	1.2	901	1180
8	0.28266	0.00003	0.00192	0.00006	0.05601	0.00147	-1.5	1.0	858	1125
9	0.28256	0.00002	0.00175	0.00003	0.05719	0.00146	-5.2	0.8	1004	1329
10	0.28261	0.00004	0.00192	0.00004	0.05958	0.00194	-3.2	1.7	927	1218
11	0.28267	0.00009	0.00379	0.00011	0.12160	0.00530	-1.2	3.2	883	1106
12	0.28262	0.00003	0.00237	0.00002	0.07819	0.00088	-2.9	1.2	926	1203
13	0.28257	0.00002	0.00107	0.00001	0.03208	0.00055	-4.5	1.0	960	1291
14	0.28265	0.00003	0.00301	0.00006	0.09508	0.00152	-1.9	1.1	898	1148
15	0.28260	0.00006	0.00265	0.00004	0.08080	0.00128	-3.6	2.1	963	1245
16	0.28261	0.00003	0.00327	0.00003	0.10860	0.00172	-3.3	1.3	965	1228
17	0.28277	0.00009	0.00280	0.00005	0.09304	0.00218	2.3	3.2	718	915
18	0.28263	0.00003	0.00277	0.00005	0.08938	0.00166	-2.6	1.3	923	1188

## 15QLR-4

1	0.28248	0.00003	0.00114	0.00002	0.03523	0.00090	-7.8	1.1	1097	1478
2	0.28254	0.00002	0.00091	0.00001	0.02699	0.00023	-5.8	0.9	1011	1366
5	0.28255	0.00003	0.00090	0.00002	0.02714	0.00061	-5.2	1.1	985	1331
6	0.28252	0.00003	0.00095	0.00001	0.03004	0.00018	-6.6	1.1	1041	1407
8	0.28259	0.00003	0.00112	0.00002	0.03331	0.00115	-3.9	1.1	939	1259
10	0.28248	0.00003	0.00100	0.00001	0.02951	0.00041	-7.7	1.1	1087	1470
12	0.28257	0.00003	0.00119	0.00009	0.03363	0.00225	-4.6	1.1	970	1301
13	0.28255	0.00003	0.00107	0.00002	0.03260	0.00076	-5.2	1.2	992	1334
15	0.28254	0.00003	0.00158	0.00003	0.04608	0.00103	-5.7	1.3	1022	1360
16	0.28248	0.00002	0.00119	0.00001	0.03762	0.00053	-7.8	1.0	1096	1475
18	0.28259	0.00004	0.00075	0.00002	0.02233	0.00061	-3.9	1.4	932	1260

19	0.28252	0.00003	0.00119	0.00001	0.04097	0.00066	-6.4	1.1	1042	1400
21	0.28253	0.00003	0.00109	0.00001	0.03306	0.00049	-6.2	1.1	1029	1385
22	0.28247	0.00002	0.00103	0.00001	0.03011	0.00041	-8.0	0.9	1101	1488
24	0.28250	0.00002	0.00157	0.00003	0.05322	0.00096	-7.1	1.0	1079	1438
25	0.28255	0.00003	0.00105	0.00001	0.03470	0.00040	-5.5	1.2	1001	1348
15QLM-37										
1	0.28253	0.00003	0.00122	0.00001	0.05070	0.00072	-5.9	1.1	1023	1372
2	0.28254	0.00002	0.00088	0.00001	0.03626	0.00037	-5.5	0.9	1001	1353
3	0.28254	0.00003	0.00099	0.00000	0.04324	0.00064	-5.5	1.1	1003	1352
5	0.28253	0.00002	0.00096	0.00000	0.03782	0.00055	-6.0	0.9	1020	1376
9	0.28261	0.00006	0.00141	0.00013	0.04950	0.00465	-3.1	2.2	916	1217
10	0.28252	0.00002	0.00079	0.00001	0.03051	0.00085	-6.3	0.9	1027	1392
13	0.28254	0.00003	0.00114	0.00001	0.04369	0.00046	-5.6	1.3	1008	1353
14	0.28257	0.00002	0.00152	0.00012	0.05989	0.00457	-4.6	0.9	979	1301
15	0.28255	0.00002	0.00083	0.00001	0.03356	0.00031	-5.1	0.9	983	1328
16	0.28259	0.00003	0.00124	0.00001	0.04183	0.00056	-3.8	1.1	940	1256
17	0.28255	0.00003	0.00119	0.00001	0.04346	0.00040	-5.2	1.1	996	1335
18	0.28265	0.00004	0.00190	0.00001	0.06699	0.00082	-1.7	1.4	867	1137
19	0.28259	0.00003	0.00183	0.00003	0.06751	0.00092	-4.0	1.0	961	1267
20	0.28255	0.00002	0.00099	0.00001	0.03692	0.00099	-5.4	1.0	1000	1347
21	0.28253	0.00003	0.00133	0.00002	0.04338	0.00064	-6.0	1.2	1031	1379